Impact of Raman Crosstalk and Relative Intensity Noise Transfer on RF Overlay in Optical Passive Networks

Hong Feng Yang

A Thesis

in

The Department

of

Electrical and Computer Engineering

Presented in Partial Fulfillment of the Requirements
for the Degree of Master of Applied Science(Electrical Engineering) at
Concordia University
Montreal, Quebec, Canada

June 2007

Your file Votre référence
ISBN: 978-0-494-34470-5
Our file Notre référence
ISBN: 978-0-494-34470-5

ABSTRACT

Impact of Raman Crosstalk and Relative Intensity Noise Transfer on RF Overlay in Optical Passive Networks

Hong Feng Yang

In the thesis, we investigate and analyze the impact of Raman crosstalk and RIN transfer on RF video overlay channels induced by 1490-nm optical intensity modulated digital data channel, considering modulation formats of non-return-to-zero (NRZ), return-to-zero (RZ), Inverse-RZ (IRZ), and Manchester coding, fiber length, optical power, optical modulation index and fiber polarization mode dispersion (PMD).

Firstly, carrier to noise ration (CNR) degradation due to the worst and best Raman crosstalk due to the Raman crosstalk is compared for NRZ, RZ, inverse RZ and Manchester. It is found that Raman crosstalk is reduced significantly when inverse RZ or Manchester is used, in contrast to NRZ and RZ.

By comparing the result of CNR degradation in a real fiber with PMD, it is found that orthogonal polarization state setting at fiber input is still helpful in the reduction of Raman crosstalk for NRZ and RZ, but hardly for inverse RZ and Manchester, if fiber length is less than 15 km, and otherwise useless due to PMD of fiber.

Also, relative intensity noise (RIN) transfer induced CNR degradation is analyzed and is too small to be considered.

ACKNOWLEDGMENTS

First of all, I would like to express my sincere gratitude to my research supervisor Professor John Xiupu Zhang for his guidance in this thesis. His support and valuable suggestion during my graduate study at Concordia University have helped me keep progressing, and made this thesis possible.

I also should give my great thanks to Frank Effenberger, the author of "Raman crosstalk control in passive optical networks", OFC Anaheim CA, Paper NWD6, 2006, and Fred Coppinger, the author of "RF video overlay in an Ethernet passive optical network," OFC Anaheim CA, Paper OThK7, 2006OFS, for providing their research presentation materials.

Learning together with other members in fiber optic communication system field has greatly enriched my education and life. I would like to thank all of them for their support and encouragement: Gino Masella and Mahmoud Alaogle. Their suggestions made the task of research enjoyable.

Finally, but not at least, I would like to thank my wife, and my parents. Their love and encouragement made me overcome difficulties and complete this degree.

TABLE OF CONTENTS

List of Figures

List of Tables

Acronyms

AM-VSB	amplitude modulation with vestigial sideband modulation
BPON	broadband passive optical network
CATV	community antenna television
CW	continuous wave
CWDM	coarse wavelength division multiplexing
CNR	carrier to noise ratio
CSO	composite second order beat
CTB	composite third order beat
DFB	distributed feedback
DSL	digital subscriber line
EDFA	erbium-doped fiber amplifier
EPON	Ethernet passive optical network
ER	extinction ratio
FRA	fiber Raman amplifier
FTTP	fiber to the premises
FWM	four-wave-mixing
GPON	gigabit capable passive optical network
GVD	group velocity dispersion

HFC	hybrid fiber-coaxial
IRZ	inverse return-to-zero
NRZ	non-return-to-zero
NTSC	national television system committee
OLT	optical line terminal
(O)MI	(optical) modulation index
PMD	polarization mode dispersion
PON	passive optical networks
PSD	power spectrum density
RF	radio frequency
RIN	relative intensity noise
RZ	return-to-zero
SBS	stimulated Brillouin scattering
SCM	sub-carrier modulation
SMF	single mode fiber
SPM	self-phase modulation
SRS	stimulated Raman scattering
TDM	time-division multiplexed
WDM	wavelength division multiplexing
WiMAX	worldwide interoperability for microwave access
XPM	cross-phase modulation

Special Symbols

$A_{channel}$	Signal amplitude per RF channel
A_{eff}	Fiber effective area
a_p	Cross-sectional area of the pump beam inside a fiber.
B	Effective noise bandwidth of each subcarrier channel at the receiver
D	Dispersion coefficient of fiber
$G(f)$	PSD of optical digital data
g_R	Effective Raman coefficient
I_m	Modulation current of directly modulated laser
I_{bias}	Laser bias of directly modulated laser
I_{th}	Laser threshold current of directly modulated laser
m_{RF}	Optical modulation index (OMI) of optical RF overlay channel
P_d	Optical power of digital data channel
P_{RF}	Optical power of RF overlay channel
P_{d0}	Average optical power of optical digital data channel
P_{RF0}	Average optical power of optical RF overlay channel
P_N	Normalized optical power of the optical digital data signal
P_r	Average received optical power of RF overlay channel
R	Detector responsivity of receiver
R_d	Data rate of digital data channel

T_{laser}	Driver transconductance of laser.
v_d	Group velocity of optical digital data channel in the fiber
v_{RF}	Group velocity of optical RF overlay channel in the fiber
z	Fiber length
α	Fiber loss
$\Delta\tau$	GVD walk-off of fiber
ε	Optical extinction ratio
λ	Wavelength
λ_d	Wavelength of digital data channel
λ_{RF}	Wavelength of digital data channel
ρ_{SRS}	Polarization overlap factor

CHAPTER 1 INTRODUCTION

1.1 Evolution of Optical Fiber Communication

Fiber-optical communication systems are concerned with lightwave systems which transmit information signals through optical fibers. Such systems have been widely deployed throughout the world since 1980, and have deeply revolutionized the telecommunication technology. The modern fiber-optic communications started around 1970s when GaAs semiconductor laser was invented, and the optical fiber loss was reduced to 20dB/km in the wavelength region near 1μm [1]. Since then, fiber-optic communication has been rapidly developed. The enormous progress of lightwave systems can be grouped into several generations. Fig. 1.1 shows the increase of bit rate-distance product over the development of lightwave systems. These data were quantified through various laboratory experiments.

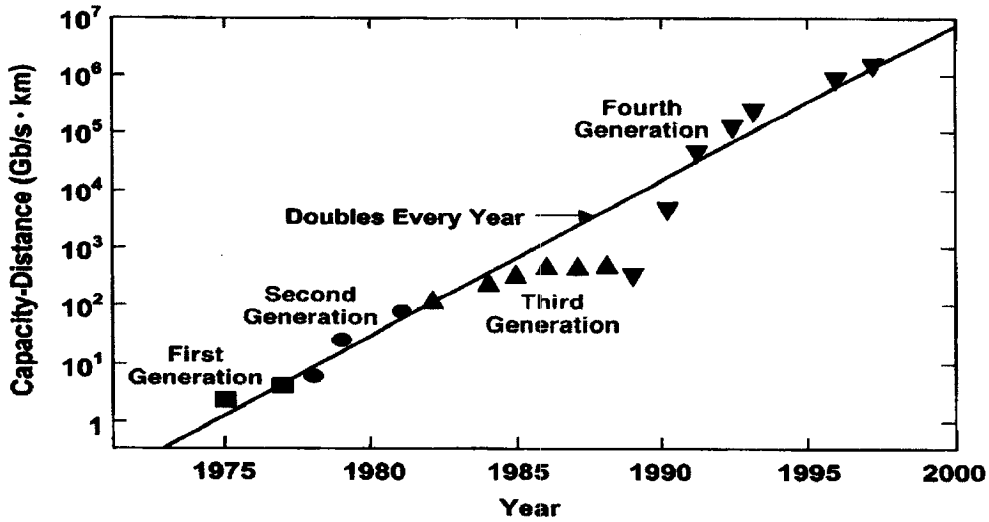

Fig. 1.1 - Increase in bit rate-distance product (BL) product over the development of

lightwave systems. Different symbols are used to distinguish each generation [2].

The first generation of lightwave systems was commercially available in 1980. It was operated near 800 nm. GaAs semiconductor lasers were also used. The data rate of the lightwave systems was around 45 Mb/s with a repeater spacing of up to 10 km.

The second generation of lightwave systems with data rate of 1.7 Gb/s and a repeater spacing of 50 km became commercially available by 1987. It was operated in the wavelength region near 1.3μm, where fiber loss was below 1 dB/km. Also, Single Mode Fiber (SMF) was first used and had exhibited a minimum dispersion in this region.

The third-generation lightwave systems with data rate of 2.5 Gb/s became commercially available in 1990. It is known that silica fibers had the minimum loss (0.2-dB/km) near the wavelength at 1.55μm. To compensate for the large fiber dispersion near 1.55μm, dispersion-shifted fiber and single-longitudinal-mode lasers were developed.

Instead of periodically using electronic repeaters with a typical spacing of 60-70 km in the third-generation lightwave systems, optical amplifiers were used in the fourth-generation lightwave systems to increase the repeater spacing and wavelength-division multiplexing (WDM) to increase capacity. Erbium-doped fiber amplifiers (EDFA) were developed in 1985 and were commercially available in 1990. EDFA made it possible to transmit optical signals up to tens of thousands of kilometer without using electronic regenerators. The advent of WDM technique started a revolution

and increased the capacity of lightwave systems enormously.

The next generations of lightwave systems, i.e. the fifth-generation of lightwave systems, have been under development for a while. The emphasis of research can be commonly categorized into two groups. One emphasis is to extend the wavelength range to L-band (1570nm – 1610nm) and S-band (1485nm – 1520nm) to increase the number of channels in WDM. Currently, lightwave systems are operated in the conventional wavelength window, known as C-band, which is from 1530 nm to 1565 nm. The other emphasis is to increase the data rate of each channel. Many experiments have been done at data rate of 10 Gb/s or 40 Gb/s per channel since year 2000. In such higher data rate lightwave systems, dispersion compensation management and combating of fiber nonlinearity induced effects like self-phase modulation (SPM), cross-phase modulation (XPM) and four-wave-mixing (FWM) are becoming critical. For this issue, modulation format has been a key factor.

1.2 Fiber Optical Networks

From an architecture standpoint, optical networks can be divided into several broad categories. Since networks may cover a small geographical area or spread over an entire continent, it is useful to classify them into three groups named as local area networks (LANs), metropolitan-area networks (MANs), and wide-area networks (WANs) according to their coverage area. An alternative classification used by the telephone industry refers to LANs as access networks, MANs as metro networks, and WANs as

transport networks [3]. In optical networks, WANs include long-haul networks and backbone networks. Fig. 1.2 illustrates four generic categories of optical networks [4].

- Long-haul networks, which span hundreds to thousands of kilometers, can transmit signals among cities or geographical regions.
- Backbone networks describe a high-capacity network that connects multiple LAN, MAN, or WAN segments, and handles inter-network traffic.
- Metropolitan networks connect groups of central offices within a city or a local geographical region. For this type of network, the distances between central offices range from a few to several tens of kilometers.
- Access networks connect a central communication office to individual business, organizations and homes.

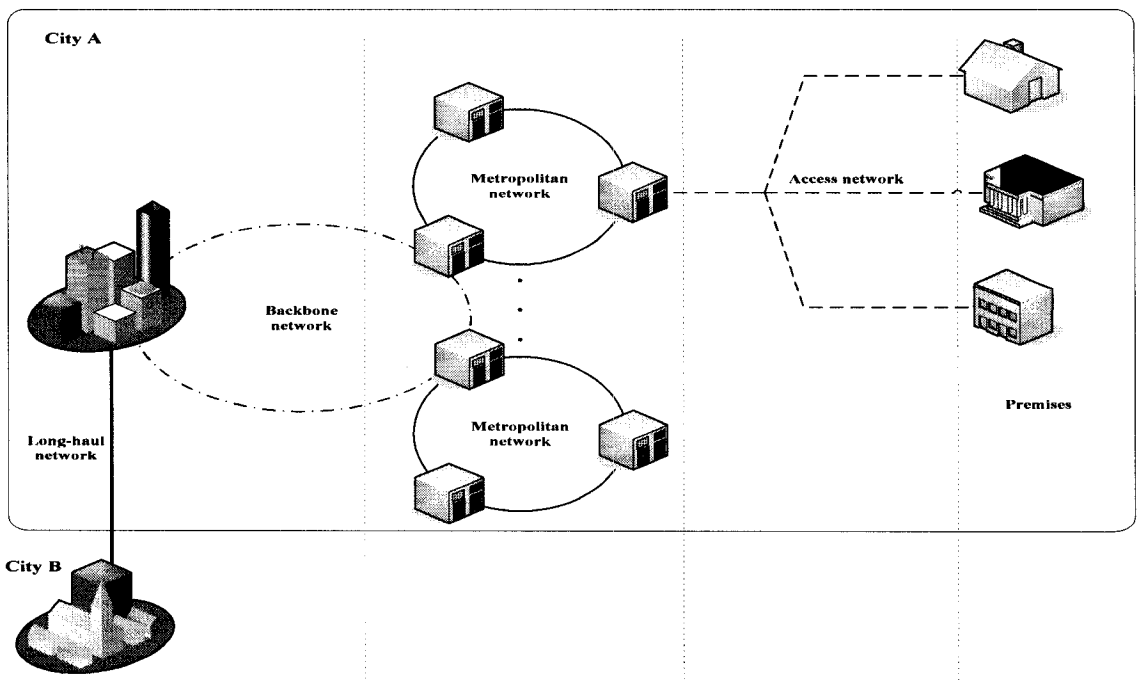

Fig. 1.2 - Overview of optical networks.

Several different wire line and wireless technologies have been used for high-capacity links in access networks. They are hybrid fiber-coax (HFC) schemes, digital subscriber lines (DSL), broadband wireless links (WiMAX), and passive optical networks (PON). The access networks are the topic of interest for PON applications. The application of PON technology, which provides broadband connectivity in the access network to homes, multiple-occupancy units, and small businesses, is commonly called fiber-to-the-premise (FTTP).

1.3 Description of Passive Optical Networks (PON)

An FTTP network can use three kinds of deployment scenarios. They are point to point topology, curb-switched network, and passive optical network (point to multipoint network).

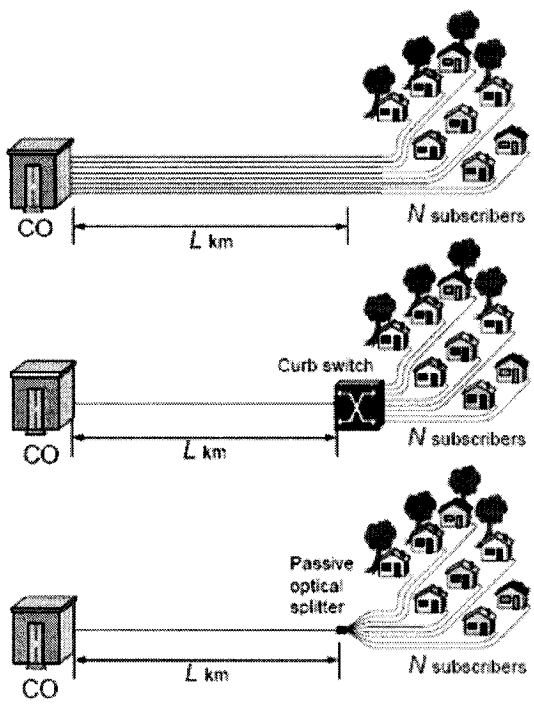

(a) Point-to- point links
- N fiber lines
-2 N transceivers

(b) Concentration switch in the neighborhood
+ 1 fiber line
- Power in the field
-2 N + 2 transceivers

(c) PON - a distributed switch
+ 1 fiber line
+ N + 1 transceivers
+ Path transparency

Fig. 1.3 - Typical FTTP architectures [5].

Shown in Fig. 1.3 (a), a straightforward way to deploy optical fiber in the local access network is to use a point-to-point (P2P) topology. Considering N subscribers, it will require NxL total fiber length and 2N transceivers with P2P architecture. It is cost prohibitive because it requires more fiber line as well as equipments space in the center office than the other two architectures (b) and (c).

Shown in Fig. 1.3 (b), in order to reduce fiber lines, a remote curb switch is deployed close to the neighborhood. This will reduce fiber consumption at the trunk line, but will increase the number of transceivers to 2N+2. What's more, a curb-switch requires electric power at the remote site.

Shown in Fig. 1.3 (c), a newly access technology called passive optical network (PON) comes out. With this technology, the active curbside switch is replaced with a passive optical splitter. PON generally consists of an OLT (Optical Line Termination), which is connected to ONUs (Optical Network Units), using only fiber cables, optical splitters and other passive components. Shown in Fig. 1.3 (c), a PON configuration reduces the amount of fiber and central office equipment required compared with concentration switch and point to point architectures. This PON architecture requires only N+1 transceivers and one fiber link.

Passive Optical Network is a high bandwidth point to multipoint (P2MP) optical fiber network based on the asynchronous transfer mode protocol (ATM), Ethernet, TDM, or

WDM.

PON uses a single port at the Central Office/Head End (CO/HE) to serve up to n subscribers through a 1 to n optical splitter. The split ratio of the splitter is typically 32, 16, or 8. Voice, data, IP video, and CATV video can all be supported on a PON by using Coarse Wavelength Division Multiplexing (CWDM). A typical PON architecture is shown in Figure 1.4

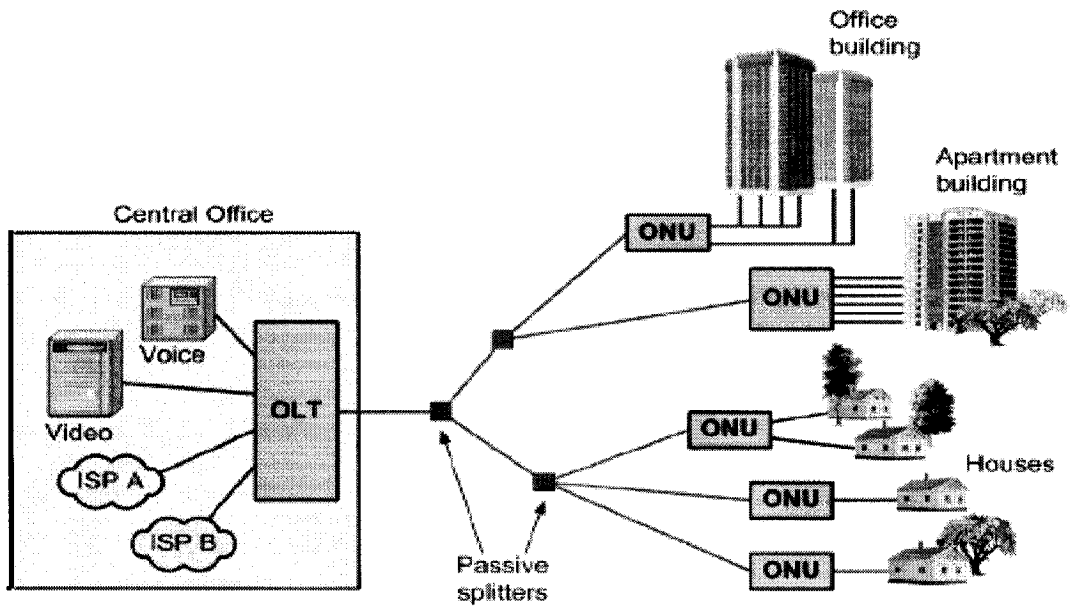

Fig. 1.4 - Passive optical networks structure [6].

1.3.1 PON Standards

Three standards have been proposed to define PON architectures. They are ITU-T G.983 series, ITU-T G.984 series, and IEEE-802.3ah standard, which define broadband PON (BPON), gigabit capable PON (GPON) and Ethernet PON (EPON), respectively.

Shown in Table 1.1, BPON system uses ATM cell to transmit downstream data at a

speed of 155.52, 622.08, and 1244.16 Mb/s. GPON system uses up to 2488.320 Mb/s downstream. However, EPON is the only access network architecture that inherits from computer networks rather than public communication network [6]. EPON has the same bite rate of 1.25 Gb/s in downstream and upstream. For all PON system, the split ratio is typically 32.

Table 1.1 PON standards- key optical specifications

Type	Data rate and reach	Split ratio	Standard	Fiber type
BPON Broadband Passive Optical Network	**Downstream: 1244, 622 or 155Mb/s Upstream:155Mb/s Max reach:20km**	**32**	**ITU G.983.3 2001**	**Single mode ITU G.652c/d (low or zero water peak) ITU G.652(std SMF)**
GPON Gigabit capable Passive Optical Network	**Downstream: 2.488 or 1.244Gb/s Upstream: 622 or 155Mb/s Max each:20km(60km)**	**32(64)**	**ITU G.984.2 2004**	**Single mode ITU G.652c/d (low or zero water peak) ITU G.652(std SMF)**
EPON Ethernet Passive Optical Network	**Downstream:1.25Gb/s Upstream:1.25Gb/s 1000BASE-PX10 10km 1000BASE-PX20 20km**	**16 or 32**	**IEEE802.3ah**	**Single mode ITU G.652c/d (low or zero water peak) ITU G.652(std SMF)**

The analysis has shown that BPON, GPON, and EPON networks can support a 20 km fiber reach with 1:32 split ratio. Also it can provide triple play services by using CWDM. In this PON architecture, the downstream digital signal can be transmitted from the OLT to the subscribers at 1490 nm using Time Division Multiplexing (TDM), and a broadcast video overlay that uses the same radio frequency technology employed in CATV HFC systems is added to PON at around 1550 nm. This 1550 nm RF signal is transmitted in a form of sub-carrier modulation (SCM) AM-VSB analog signal, which can carry analog channels and digital channels.

Shown in Table 1.2, while the protocols of these three systems are quit different, they all share the same wavelength plan that uses the 1480-1500nm wavelength range for downstream data signal, the 1260-1360nm wavelength range for upstream, and the enhancement band of 1550-1560nm for video distribution service. Due to the fact that CATV RF video overlay is analog based transmission, the CATV RF signals are very sensitive to any crosstalk and distortion.

Table 1.2 Wavelength allocation of PON

Items	Notation	Unit	Nominal value	Application examples
1.3 μm wavelength band				**For use in ATM-PON upstream.**
Lower limit	**–**	**nm**	**1260**	
Upper limit	**–**	**nm**	**1360**	
Intermediate wavelength band				**For future use Reserved band including guardbands for allocation by ITU-T.**
Lower limit	**–**	**nm**	**1360**	
Upper limit	**λ1**	**nm**	**1480**	
Basic Band				**For use in ATM-PON downstream.**
Lower limit	**λ1**	**nm**	**1480**	
Upper limit	**λ2**	**nm**	**1500**	
Enhancement Band (Option 1)				**For additional digital service use.**
Lower limit	**λ3**	**nm**	**1539**	
Upper limit	**λ4**	**nm**	**1565**	
Enhancement Band (Option 2)				**For video distribution service.**
Lower limit	**λ3**	**nm**	**1550**	
Upper limit	**λ4**	**nm**	**1560**	
Future L Band				**For future use Reserved band for allocation by ITU-T.**
Lower limit	**λ5**	**nm**	**For further study**	
Upper limit	**λ6**	**nm**		

1.4 Description of Several Important Definitions

1.4.1 Raman scattering

Spontaneous Raman scattering was first discovered by Raman, for which he received the Nobel Prize in Physics in 1930 [7]. It occurs in optical fibers when the pump light is scattered by the molecules of silica. The energy diagram shown in Figure 1.5 can describe the energy-level diagram of Raman scattering. There are basically two types of Raman scattering process [8],

- Absorption of a pump photon followed by a change in vibrational energy of the participation molecule and the emission of a photon with the energy difference. This is called Stokes scattering.

- If the pump photon is absorbed by a molecule that is already excited, a photon with energy equal to the sum of energies is emitted. This is called anti-Stokes scattering. It only takes place for a fiber temperature above the absolute zero – non-zero population of the excited vibrational state is needed.

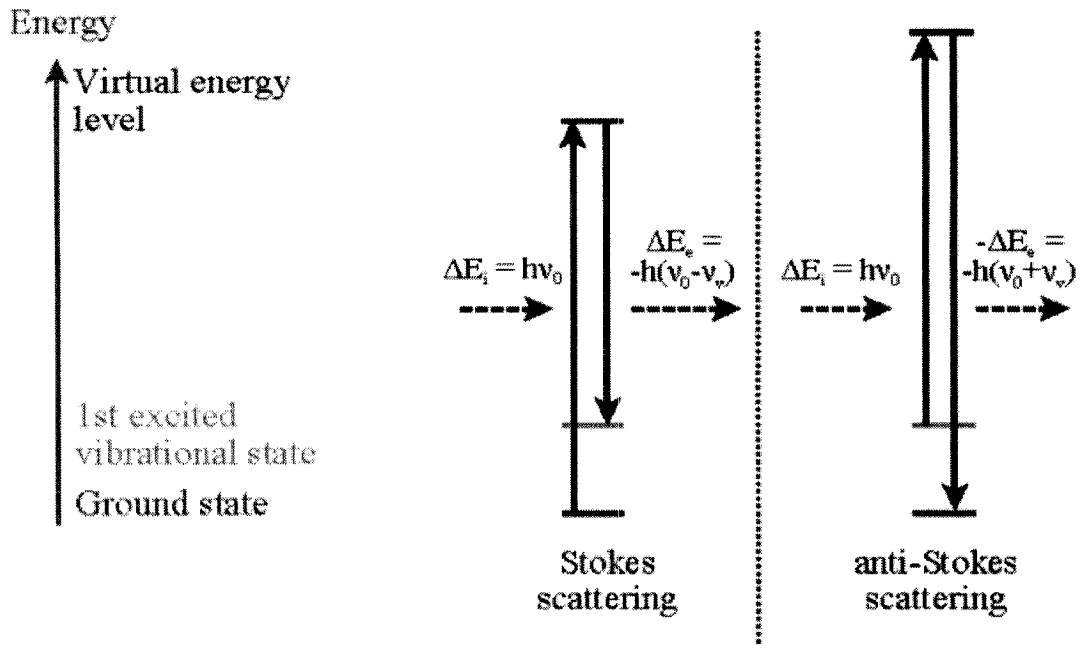

Fig. 1.5 - Energy diagram for the Raman scattering processes: Stokes scattering and anti-Stoke scattering [8].

The Raman scattering process becomes stimulated if the pump power exceeds a threshold value [9]. Stimulated Raman Scattering (SRS) can occur in both the forward and the backward directions in optical fibers.

1.4.2 Raman amplification

In a quantum mechanical description, shown in the energy-level diagram in Figure1.6, a pump photon is converted into a second signal photon that is an exact replica of the first, and the remaining energy produces an optical phonon. The initial signal photon, therefore, has been amplified.

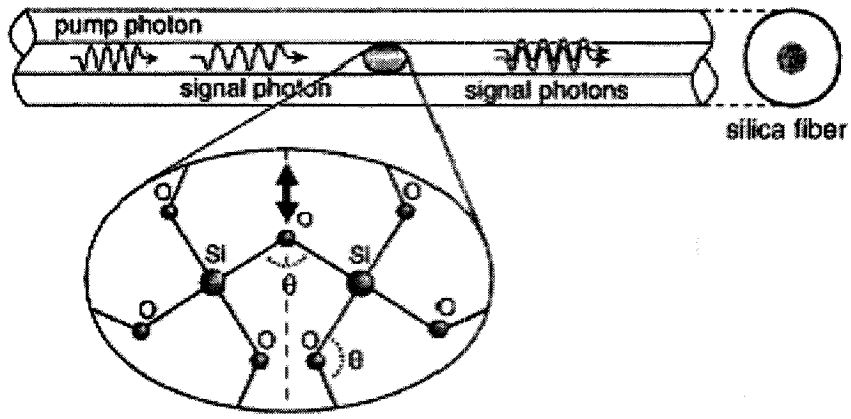

Fig. 1.6 - Schematic depicting amplification by SRS in an optical silica fiber. The silica molecules convert the pump into a replica of the signal photon, producing an optical phonon [8].

The Raman gain coefficient is a fundamental parameter for Raman amplification. This parameter determines the strength of the coupling between a pump beam and a signal beam due to SRS. The Raman–gain coefficient g_R is related to the optical gain $g(z)$ as $g = g_R I_p(z)$, where I_p is the pump intensity. In terms of the pump power P_p, the gain can be written as

$$g(\omega) = g_R(\omega)(P_p / a_p) \tag{1.1}$$

Here, a_p is the cross-sectional area of the pump beam inside a fiber. Since a_p can vary considerably for different types of fibers, the ratio g_R/a_p is a measure of the Raman-gain efficiency. The ratio when pump and signal are co-polarized (solid curve) or orthogonally polarized (dotted curve) is plotted in Figure 1.7.

1.4.3 Raman crosstalk in PON RF video overlay channel

When a 1550 nm video overlay signal is transmitted in a PON system, one of the most important issues we must consider is that downstream data transmission at the 1490nm wavelength from OLT can cause Stimulated Raman Scattering (SRS) induced noise in the 1550nm video overlay signal. This noise can result in reduced carrier to noise ratio (CNR) if the 1490nm power exceeds certain limits.

These Raman scattering processes can cause noise if signal photons having photon energies within the Raman line are injected together with a strong co-polarized pump [8]. Shown in Fig. 1.7, very small Raman crosstalk takes place if the signal and pump are launched in orthogonal polarizations.

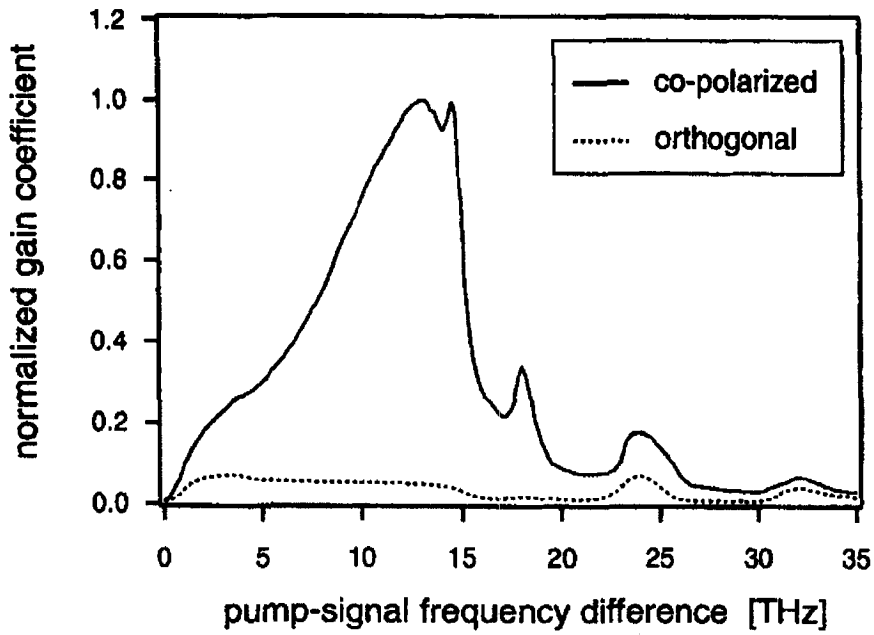

Fig. 1.7 - Raman-gain coefficient (peak value normalized to 1) when pump and signal are co-polarized (solid curve) or orthogonally polarized (dotted curve) [8].

The Raman scattering spectrum of the data signal at 1490 nm will act as an additional noise to the video signal at 1550 nm. The spectrum of Raman gain has a peak at 13.5THz (~100 nm) when pump light works at 1490 nm. Thus, at the wavelength difference of 60nm (difference from 1550nm to 1490nm), the Raman gain is still high enough to affect the RF channel.

1.4.4 Polarization Mode Dispersion

The Polarization Mode Dispersion (PMD) results from the fact that light-signal energy at a given wavelength in a single-mode fiber actually occupies two orthogonal polarization states or modes. Fig. 1.8 shows this condition. At the start of the fiber, the two polarization states are supposed to be aligned. However, because of fiber birefringence, the refractive index of optical fiber material is not perfectly uniform across any given cross-sectional area , and varies along the length of fiber; Consequently, each polarization mode will encounter a slightly different propagation velocity so that one polarization mode will travel faster and limit the performance of modern lightwave systems.

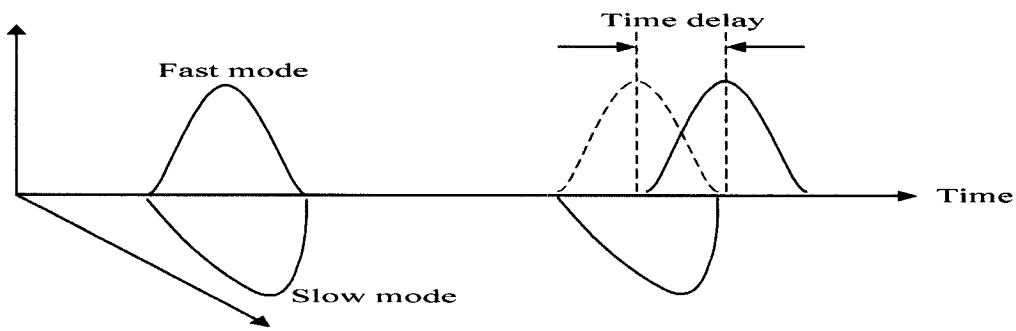

Fig. 1.8 - Variation in the polarization states of an optical pulse because of PMD.

It is well known that Raman crosstalk between any two optical channels is strongly dependent on polarization states of the two optical channels along a fiber. In PON systems, Raman crosstalk from the 1490-nm optical digital data channel to the 1550-nm optical RF overlay channel is thus dependent on polarization states of the two optical channels along a fiber, and is in turn dependent on the input polarization states of the two optical channels and polarization mode dispersion (PMD) of the transmission fiber. Therefore, it is found that the worst Raman crosstalk is hard to be estimated experimentally due to inevitable fiber PMD [10]. On the other hand, PMD, in average, reduces Raman crosstalk due to random nature of PMD [11].

In the simulation, we set correlation length to 50m, i.e. the continuous variations of birefringence are substituted by series of many short sections of 50m with constant birefringence. It is said to be coarse step method in PMD analysis. The axis of local birefringence varies from section to section. It means that polarization state of the optical field is scattered to a new point as shown in Fig. 1.9.

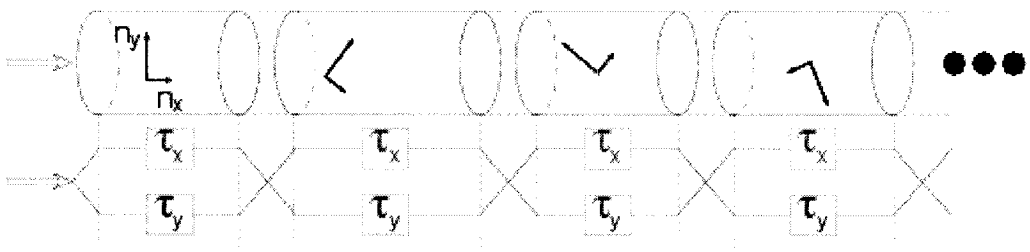

Fig. 1.9 - Schematic representation of coarse step method.

1.4.5 PON RF Video Overlay Design Considerations

RF Video overlay transmission equipment employed for FTTP is typically used for CATV HFC system. The RF video overlay typically deployed 80 analog channels from 50 to 550MHz, and potentially many additional digital channels using sub-carrier multiplexing with 64-QAM or 256-QAM. To achieve good picture quality for this case, there are three requirements that must be met at the receiver.

- Carrier to Noise Ratio (CNR) is the key parameter. It must above 44dB to meet FCC requirements and above 47dB to eliminate noticeable video "snow".
- Composite Second Order distortion (CSO) should be less that -54dBc to avoid swimming diagonal stripes in the video.
- Composite Triple Beat distortion (CTB) should be less than -54dBc to avoid horizontal line in the video.

With standard RF video transmission system at 20km distance, the critical parameter to manage is CNR. In this case, if CNR is above 47dB, the CSO and CTB requirements are easily met.

◆ **CNR (Carrier to Noise Ratio) Calculation**

To measure CNR we use a module, which allows automated measurement of the ratio of powers falling within two filtered bandwidths. The input signal is sent to two separate filters, which have a Gaussian pass-band and a specified bandwidth. The order of the Gaussian can be specified and high orders will approximate to a brick-wall filter.

The function of the module can be expressed mathematically from the voltage outputs of the two filters v where R is the output of the module,

$$R(dB) = 10\log\frac{\overline{v^2_{Filter1}}}{\overline{v^2_{Filter2}}} \qquad (1.2)$$

The ratio of the output powers of the carrier and noise filters is calculated and converted to dB. A ratio of 10 in power gives an output of 10 dB.

◆ CSO (Composite Second Order Beat) and CTB (Composite Third Order Beat) Calculation

CSO is defined as the ratio of carrier to Composite Second Order Beat and CTB is the ratio of carrier to Composite Third Order Beat. Both of them are the result of multiple carriers experiencing second and third order non-linearity and so generating multiple distortion products.

These products are measured as a group thus the term composite distortion as opposed to discrete distortion. The CTB products fall close to the carriers because of the choice of equally spaced carrier frequencies. Second order distortion products fall +/- 1.25 MHz from each carrier. A small quantity of the second order products fall 0.75 MHz from some carriers.

For NTSC systems, the CSO intermodulation products are displaced from the carriers by +/-1.25 MHz as shown in Fig. 1.10.

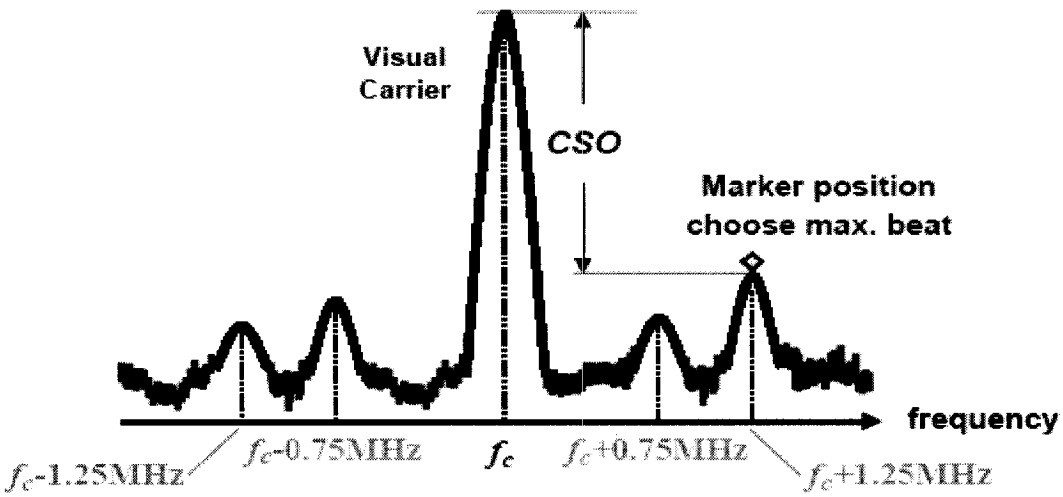

Fig. 1.10 - Frequency position of CSO and visual carrier [12].

The power difference between visual carrier and noise level at 1.25MHz from it is the CSO distortion.

Because the major components of CTB fall on the frequencies of the carriers, CTB distortion must be measured by turning off the appropriate channel carrier as shown in Fig. 1.11 [12].

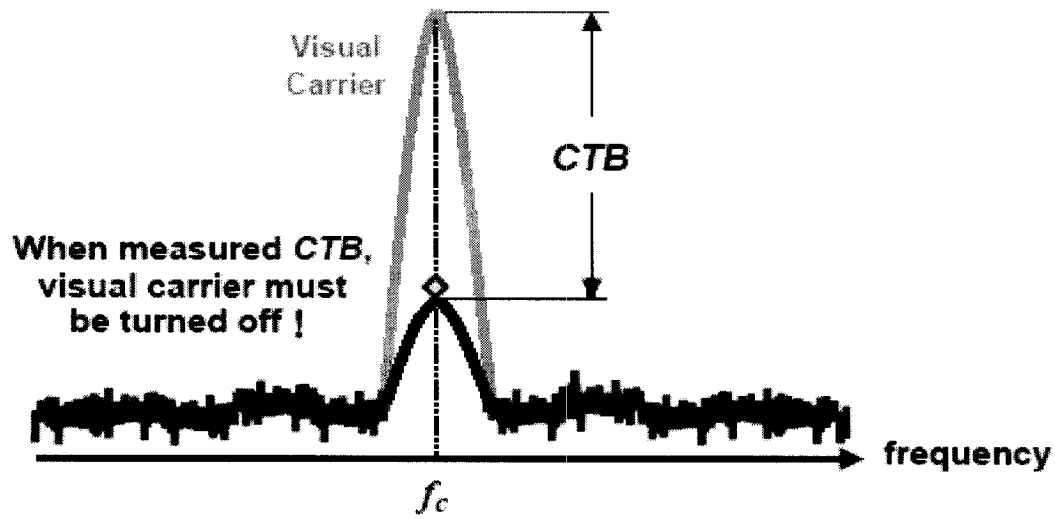

Fig. 1.11 - Frequency position of CTB and visual carrier [12].

The power difference between visual carrier and noise level when visual carrier is off is the CTB distortion.

1.4.6 Noise Contributions

Thermal Noise, shot noise from photo-diode, Relative Intensity Noise (RIN) from lasers, and clipping noise from lasers are the typically four kinds of dominant noise in SCM systems. Each is described as follows.

Thermal Noise is generated in resistive elements of the link including the photo-diode and the modulator. Its mean square current value is given by

$$\left\langle I_{th}^2 \right\rangle = \left(\frac{4 \cdot K \cdot T \cdot B}{R}\right) \qquad (1.3)$$

where K is Boltzmann constant, T is the absolute temperature, B is the video stream bandwidth, and R is the load resistance value. In the simulation, we set thermal noise of 7.5 $pA/\sqrt{Hz}$ at the PIN diode.

Shot Noise is generated when an optical signal is incident on the photo-detector. Its value is given by

$$\left\langle I_{shot}^2 \right\rangle = 2 \cdot q(I + I_d) \cdot B \qquad (1.4)$$

where q is the electronic charge, I is the mean optically generated current, and I_d is the photodetector dark current.

Relative Intensity Noise (RIN) is generated by spontaneous emission within the laser source. It is dependent on material, structural and modulation parameters. The contribution of the source RIN to the noise current at the detector for a CW laser is given

by

$$\left\langle I_{RIN}^2 \right\rangle = I^2 \cdot RIN \cdot B \tag{1.5}$$

Moreover, accompanying Raman crosstalk, relative intensity noise (RIN) of the 1490-nm optical digital data channel is also transferred to the 1550-nm optical RF overlay channel [13].

Clipping noise is generated when a semiconductor laser is driven below threshold by the modulating current, which is shown in Fig. 1.12. Clipping is given by

$$Clipping^{-1} = \left[\sqrt{2\pi} \frac{\left(1+6\mu^2\right)}{\mu^3} e^{\frac{1}{2\mu^2}} \right]^{-1}, \mu = m\sqrt{N/2} \tag{1.6}$$

where N is the number of SCM channels, and m is the optical modulation index per channel.

When transporting multiple signals in SCM network, the modulated composite input signal is only weakly clipped by laser so that the desirable CNR and low CTB/CSO values are obtained. Clipping sets the fundamental limitation on how much the laser can be clipped for composite input signal.

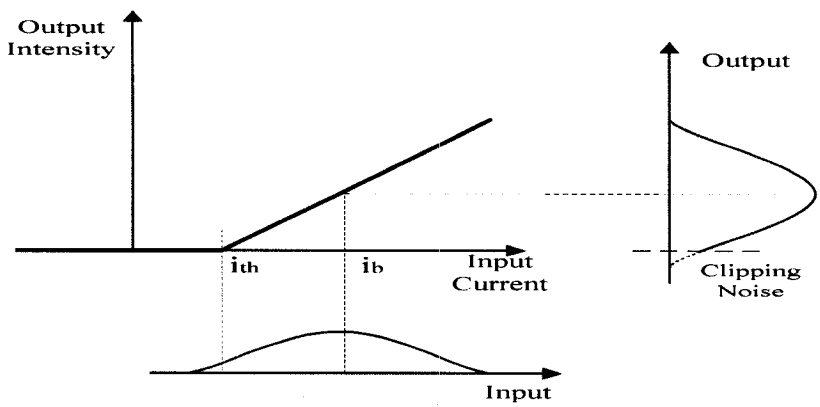

Fig. 1.12 - Generation of clipping noise.

1.4.7 Analog Modulated Video Signal

The National Television Systems Committee (NTSC) came out in 1941 and established color TV standards in 1953. It is used as terrestrial broadcasting and cable TV transmission systems in North America, Japan, and many other countries.

As shown in Fig. 1.13, the standard modulation format for NTSC analog video stream is Amplitude modulation with vestigial sideband modulation (AM-VSB). In AM-VSB each video stream was converted on an allocated CATV frequency. The NTSC standard analog video stream has two major components: video carrier and audio subcarrier.

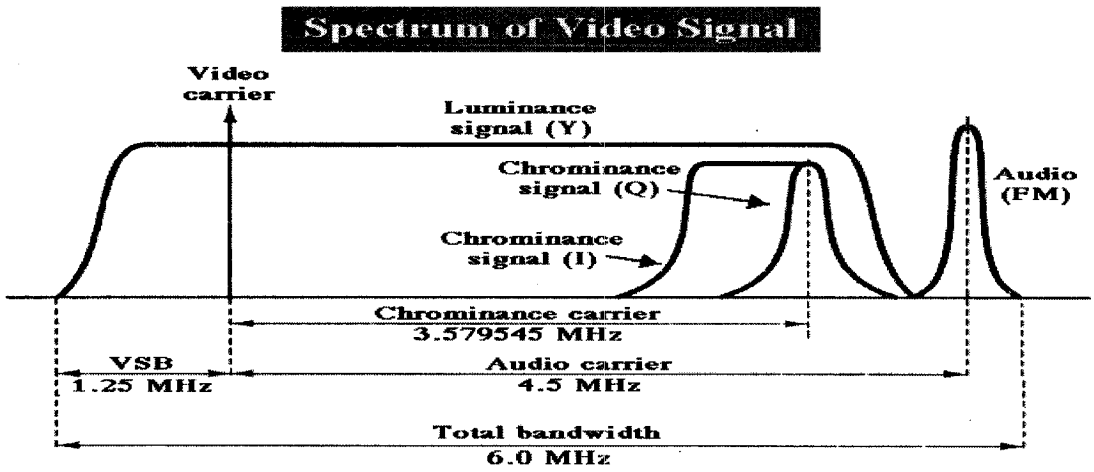

Fig. 1.13 - Spectrum of NTSC video signal [14].

The TV luminance and the 3.58 MHz chrominance subcarrier amplitude modulates an IF video carrier (such as 55.25MHz, 61.25MHz etc.). Then, an asymmetrically filter is used to filter portion of the upper sideband of the amplitude modulated signal such that the lower sideband edge is 1.25MHz below the IF video carrier and the upper sideband edge is 4.75MHz above the IF video carrier. The audio subcarrier is 4.5MHz above the

video carrier. The total channel bandwidth is 6.0 MHz. In NTSC, chrominance is encoded using two 3.579545 MHz signals that are 90 degrees out of phase, known as I (in-phase) and Q (quadrature) QAM. Specifications of NTSC-M is shown in Table 1.3

Table 1.3 Specifications of NTSC-M in America.

Channel bandwidth at RF (MHz)	6	Chrominance subcarrier frequency (Hz)	3,579,545 ± 10=3.58MHz
Frequency separation between video and audio carrier (MHz)	4.5	Video bandwidth (MHz)	4.2

1.4.8 Frequency Allocation Tables of NTSC

NTSC supports color television transmission in a 6-MHz channel bandwidth and has 525 interlaced scan lines. Two fields are interlaced to make one frame with a frame rate of 29.97 frames per second and a field rate of 59.94 fields per second. A fraction (approximately 8 percent) of the available bandwidth is used for signal synchronization between the transmitter and the receiver, giving an effective resolution of 640x480. The aspect ratio, or ratio of picture width to picture height, is 4:3 [14].

Table 1.4 lists the frequency band, the visual carrier frequency and the chrominance and audio subcarrier frequency for each of the 80 NTSC channels. All frequencies are in MHz. CH means channel number in the TV system; BAND means the channel band range and the bandwidth is 6MHz; VIDEO means video carrier frequency; CROMA means chrominance subcarrier frequency; and AUDIO means audio subcarrier frequency.

Table 1.4 NTSC frequency assignments (MHz)

---------- VHF ----------

CH	BAND	VIDEO	CHROMA	AUDIO
2	54- 60	55.25	58.8295	59.75
3	60- 66	61.25	64.8295	65.75
4	66- 72	67.25	70.8295	71.75
5	76- 82	77.25	80.8295	81.75
6	82- 88	83.25	86.8295	87.75
7	174-180	175.25	178.8295	179.75
8	180-186	181.25	184.8295	185.75
9	186-192	187.25	190.8295	191.75
10	192-198	193.25	196.8295	197.75
11	198-204	199.25	202.8295	203.75
12	204-210	205.25	208.8295	209.75
13	210-216	211.25	214.8295	215.75
FM				
95	90-96	91.25	94.8295	95.75
96	96-102	97.25	100.8295	101.75
97	102-108	103.25	106.8295	107.75
98	108-114	109.25	112.8295	113.75
99	114-120	115.25	118.8295	119.75

---------- CATV ----------

CH	BAND	VIDEO	CHROMA	AUDIO
14	120-126	121.25	124.8295	125.75
15	126-132	127.25	130.8295	131.75
16	132-138	133.25	136.8295	137.75
17	138-144	139.25	142.8295	143.75
18	144-150	145.25	148.8295	149.75
19	150-156	151.25	154.8295	155.75
20	156-162	157.25	160.8295	161.75
21	162-168	163.25	166.8295	167.75
22	168-174	169.25	172.8295	173.75
23	216-222	217.25	220.8295	221.75
24	222-228	223.25	226.8295	227.75
25	228-234	229.25	232.8295	233.75
26	234-240	235.25	238.8295	239.75
27	240-246	241.25	244.8295	245.75
28	246-252	247.25	250.8295	251.75
29	252-258	253.25	256.8295	257.75
30	258-264	259.25	262.8295	263.75
31	264-270	265.25	268.8295	269.75
32	270-276	271.25	274.8295	275.75
33	276-282	277.25	280.8295	281.75
34	282-288	283.25	286.8295	287.75
35	288-294	289.25	292.8295	293.75
36	294-300	295.25	298.8295	299.75
37	300-306	301.25	304.8295	305.75
38	306-312	307.25	310.8295	311.75
39	312-318	313.25	316.8295	317.75
40	318-324	319.25	322.8295	323.75
41	324-330	325.25	328.8295	329.75
42	330-336	331.25	334.8295	335.75
43	336-342	337.25	340.8295	341.75
44	342-348	343.25	346.8295	347.75
45	348-354	349.25	352.8295	353.75
46	354-360	355.25	358.8295	359.75
47	360-366	361.25	364.8295	365.75
48	366-372	367.25	370.8295	371.75
49	372-378	373.25	376.8295	377.75
50	378-384	379.25	382.8295	383.75
51	384-390	385.25	388.8295	389.75
52	390-396	391.25	394.8295	395.75
53	396-402	397.25	400.8295	401.75
54	402-408	403.25	406.8295	407.75
55	408-414	409.25	412.8295	413.75
56	414-420	415.25	418.8295	419.75
57	420-426	421.25	424.8295	425.75
58	426-432	427.25	430.8295	431.75
59	432-438	433.25	436.8295	437.75
60	438-444	439.25	442.8295	443.75
61	444-450	445.25	448.8295	449.75
62	450-456	451.25	454.8295	455.75
63	456-462	457.25	460.8295	461.75
64	462-468	463.25	466.8295	467.75
65	468-474	469.25	472.8295	473.75
66	474-480	475.25	478.8295	479.75
67	480-480	481.25	484.8295	485.75
68	486-492	487.25	490.8295	491.75
69	492-498	493.25	496.8295	497.75
70	498-504	499.25	502.8295	503.75
71	504-510	505.25	508.8295	509.75
72	510-516	511.25	514.8295	515.75
73	516-522	517.25	520.8295	521.75
74	522-528	523.25	526.8295	527.75
75	528-534	529.25	532.8295	533.75
76	534-540	535.25	538.8295	539.75

In this thesis, we use the module that generates the sum of 80 sinusoidal carriers with specified channel spacing of 6MHz at video carrier frequency of 55.25MHz, 61.25MHz etc., which is shown in Table 1.4. Each carrier is of the form,

$$v = A\sin(2\pi ft + \theta) \tag{1.7}$$

where A is the zero-peak amplitude of the carrier, f is its frequency, t is time, and θ is its phase. The phase of each subcarrier is set random phase on each iteration. That is similar to a realistic system, where the individual carriers are not phase locked. Fig. 1.14 shows the detected RF signal spectrum after photodetector.

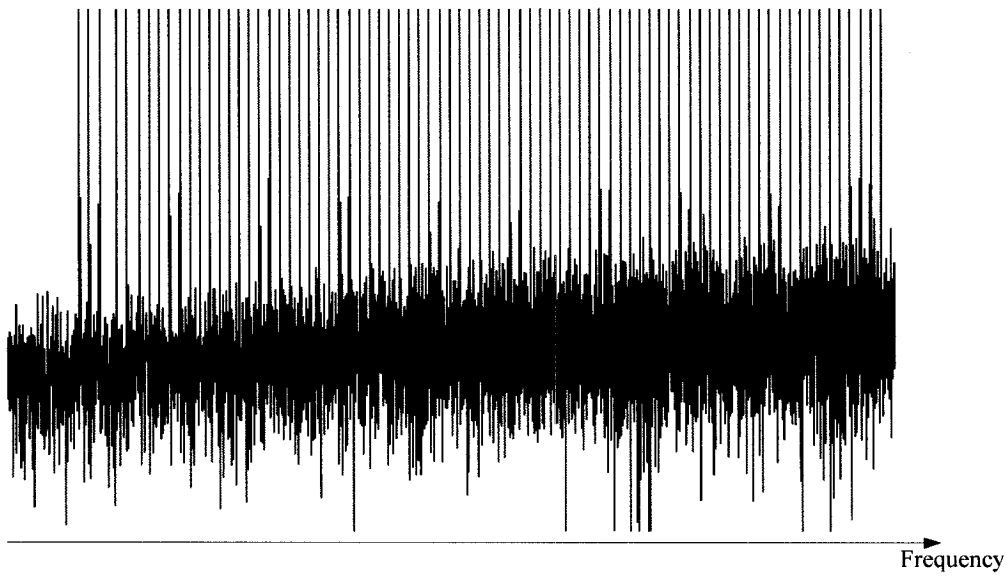

Fig. 1.14 - PIN diode output RF spectrum (80 channels)

1.5 Motivations of This Thesis

PON systems provide digital data transmission at 1490 nm, and also transport CATV RF video overlay in down stream at 1550 nm. Due to the fact that CATV RF video overlay is analog based transmission, the CATV RF signals are very sensitive to any

crosstalk and distortion. It is well known that fiber Raman effect will induce Raman crosstalk between wavelength division multiplexing (WDM) channels including hybrid WDM systems [15-16]. Many methods have been deployed to reduce the impact of the Raman crosstalk. It is found that the Raman crosstalk seriously degrades RF video channels with frequencies of in the range of 55-100 MHz, i.e. the crosstalk has a low-pass characteristic, and pre-emphasized RF power is required to meet the required CNR, specified by NTSC [17-18]. Moreover, optical baseband digital data transmission in PON systems is based on time division multiplexing packets or frames. In other words, idle frames are often sent in the absence of real traffics. By using Manchester coded binary sequences in idle patterns to shape the signal spectrum of optical intensity modulated digital data, the Raman crosstalk in the low frequency channels (channel 2 to 6) is reduced in Ethernet PON systems [19-20].

Followed by these researches in [15-20], our motivations is to investigate and analyze the impact of Raman crosstalk and RIN transfer on RF video overlay channels induced by 1490-nm optical intensity modulated digital data channel, considering modulation formats of non-return-to-zero (NRZ), return-to-zero (RZ), Inverse-RZ (IRZ), and Manchester coding, fiber length, optical power, optical modulation index and fiber PMD, and develop new solutions to reduce the Raman crosstalk in RF overlay channel of PON. The upper and lower bounds of Raman crosstalk, fiber PMD effect on Raman crosstalk, and RIN transfer induced CNR degradation will be presented.

In the past, modulation formats such as NRZ, Manchester have been present to analyze and control the impact of Raman crosstalk in PON system [19].

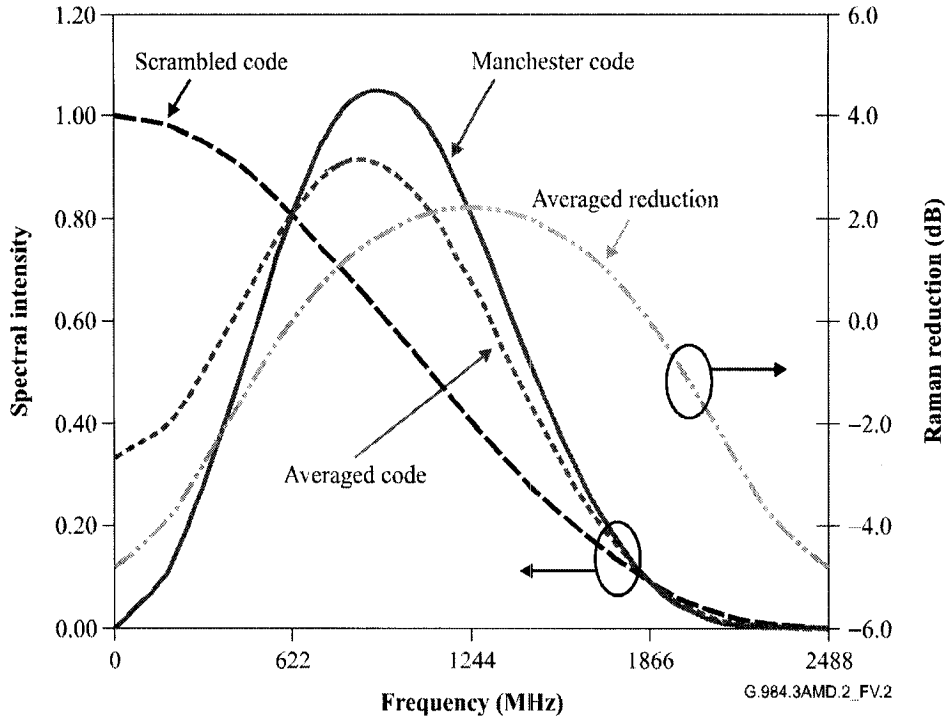

Fig. 1.15 - Digital signal spectra and Raman reduction with idle pattern control [19].

As shown in Fig. 1.15, in a typical G-PON system, there could approximately be 25% traffic on average. That is, there will be 75% idle time. In addition, the cell headers, which can not be controlled, occupy 10% of idle time. As a result, the controllable pattern appears on the line approximately 67% of the time. Therefore, the spectrum of the line signal will be the weighted average of the scrambled and Manchester coded spectra. The average reduction in spectral intensity is then as shown in Fig. 1.15. In the important 50~100 MHz region, the reduction is around 4 dB in this example [21]. This would produce a 3 dB improvement in Raman impairments for overlay signals on the PON. It

should be noted that higher downstream utilization will produce less improvement, and vice versa.

In this thesis, we investigate two new coding schemes, i.e. RZ and Inverse-RZ coding [22], to analyze the Raman effect. By comparing the CNR degradation of different digital channel coding schemes, we can get the impact of different signal spectrum of optical intensity modulated digital data.

In addition to coding schemes, optical power of digital channel and modulation index of RF overlay channels are also investigated to find the impact on the Raman crosstalk degradation. Fiber PMD impact are also considered according to different kinds of coding.

1.6 Thesis Structure

The structure of the thesis is described in this section – for each chapter the main contents are described.

In Chapter 2, we present the theory of the Raman crosstalk in PON. Firstly, the Raman crosstalk modeling is given in Section2.1. Furthermore, the PON systems under consideration are given in Section 2.2. Then, the specific simulation modules are listed in the subsections of Section 2.3.

In Chapter 3, we investigate simulations of Raman crosstalk in PON systems. Section 3.1 illustrates the low pass characteristic of Raman crosstalk at NTSC channel. Section 3.2 considers Raman crosstalk induced CNR degradation with a virtual

assumption that fiber has no PMD when polarization states of video overlay channel and digital channel maintain along the fiber with parallel and orthogonal aligned. Section 3.3 illustrates Raman crosstalk with the consideration of PMD, i.e. real fiber. For this case, we investigate CNR degradation due to Raman crosstalk if polarization states along a fiber have random evolution due to PMD. Thus, we can evaluate the PMD impact on Raman crosstalk induced CNR degradation. Finally, we evaluate RIN transfer impact on CNR in Section 3.4

In Chapter 4, we conclude this thesis and summarize all the results shown in all the previous chapters.

CHAPTER 2 MODELING OF RAMAN CROSSTALK IN PON SYSTEMS

This chapter presents the theory of the Raman crosstalk in PON systems. Firstly, the Raman crosstalk modeling is given in Section 2.1. The PON systems under the consideration are described in Section 2.2. Then, the specific modules which are used for simulation are briefed in Section 2.3.

2.1 Raman Crosstalk Modeling

A formal approach to evaluate the Raman crosstalk is to solve the coupled propagation equations of the optical power P_{RF} at a wavelength of λ_{RF} and P_d at a wavelength of λ_d along a fiber. Specifically, the optical digital data channel at λ_d is the pump of the Raman crosstalk for the optical RF overlay channel, i.e. $\lambda_d < \lambda_{RF}$ as shown in Fig. 2.1. λ_{RF} is the optical RF overlay channel wavelength and λ_d is the optical digital data channel wavelength.

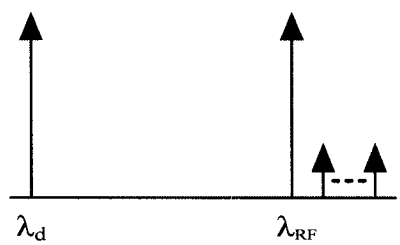

Fig. 2.1 - Wavelength allocation in modeling

The coupled equations are given by [15]

$$\frac{\partial P_{RF}}{\partial z} + \frac{1}{v_{RF}} \frac{\partial P_{RF}}{\partial t} = (g_R P_d - \alpha) P_{RF} \quad \text{for optical RF overlay channel} \qquad (2.1)$$

$$\frac{\partial P_d}{\partial z}+\frac{1}{v_d}\frac{\partial P_d}{\partial t}=\left(-g_R P_{RF}-\alpha\right)P_d \qquad \text{for optical digital data channel,} \qquad (2.2)$$

where z is the position of fiber length, α is the loss of the fiber , g_R is the effective Raman coefficient, v_{RF} is the group velocity of the optical RF overlay channel in the fiber, v_d is the group velocity of optical digital data channel in the fiber, P_{RF} is the optical RF overlay channel power and P_d is the optical digital data channel power.

Assuming no pump power depletion of the optical digital data channel due to Raman crosstalk and using τ_d to substitute t with $\tau_d = t-\frac{z}{v_d}$, we solve (2.1) and (2.2) and obtain,

$$\begin{aligned} P_d(z,\tau_d) &= P_d(0,\tau_d)e^{-\alpha z}\times\exp\left[-g_R\cdot\int_0^z \rho(z')P_{RF}(0,\tau_d+\Delta\tau\cdot z')\cdot e^{-\alpha z'}dz'\right] \\ &\approx P_d(0,\tau_d)e^{-\alpha z}\times\left[1-g_R\cdot\int_0^z \rho(z')P_{RF}(0,\tau_d+\Delta\tau\cdot z')\cdot e^{-\alpha z'}dz'\right] \end{aligned} \qquad (2.3)$$

A similar approach can be used to have,

$$\begin{aligned} P_{RF}(z,\tau_{RF}) &= P_{RF}(0,\tau_{RF})e^{-\alpha z}\times\exp\left[g_R\cdot\int_0^z \rho(z')P_d(0,\tau_{RF}+\Delta\tau\cdot z')\cdot e^{-\alpha z'}dz'\right] \\ &\approx P_{RF}(0,\tau_{RF})e^{-\alpha z}\times\left[1+g_R\cdot\int_0^z \rho(z')P_d(0,\tau_{RF}+\Delta\tau\cdot z')\cdot e^{-\alpha z'}dz'\right] \end{aligned} \qquad (2.4)$$

where the exponential is approximated to the first order, $\Delta\tau=\left|\frac{1}{v_d}-\frac{1}{v_{RF}}\right|\approx D\left|\lambda_d-\lambda_{RF}\right|$ represents the group velocity mismatch between the two channels, the factor ρ represents the polarization overlap factor with $\rho\le 1$, and D is the dispersion coefficient of the fiber.

If we set optical RF overlay channel to be a modulated wave, i.e. $P_{RF}(0,t) = P_{RF0}[1 + m_{RF}\cos(2\pi f \cdot t)]$ and the optical digital data channel to be a CW wave, i.e. $P_d(0,t) = P_{d0}$, where m_{RF} is the optical modulation index (OMI) of optical RF overlay channel, f is the RF subcarrier frequency, and P_{d0} and P_{RF0} are the average optical power of the optical digital data and RF overlay channels. To obtain an explicit expression of Raman crosstalk, we substitute those into (2.3) yields,

$$P_d(z,\tau_d) = P_{d0}e^{-\alpha z}\left[1 - \rho_{SRS}g_R\int_0^z P_{RF0}e^{-\alpha' dz'} - \rho_{SRS}g_R\int_0^z P_{d0}m_{RF}\cos\left(2\pi f\tau_d + 2\pi f\Delta\tau\cdot z'\right)\cdot e^{-\alpha' dz'}\right]$$

$$= P_{d0}e^{-\alpha z}\left\{1 - \rho_{SRS}\,g_R P_{RF0}\left|\frac{1-e^{-\alpha z}}{\alpha}\right| - \cos(2\pi f\tau_d + \Theta_{SRS})\right.$$

$$\left.\times\,\rho_{SRS}\,g_R P_{RF0} m_{RF}\,\frac{\sqrt{1+e^{-2\alpha z} - 2e^{-\alpha z}\cos(2\pi f\Delta\tau\cdot z)}}{\sqrt{\alpha^2 + (2\pi f\Delta\tau)^2}}\right\} \qquad (2.5)$$

where $\Theta_{SRS} = \tan^{-1}\left(\frac{-2\pi f\Delta\tau}{-\alpha}\right) + \tan^{-1}\left(\frac{e^{-\alpha z}\sin(2\pi f\Delta\tau\cdot z)}{e^{-\alpha z}\cos(2\pi f\Delta\tau\cdot z) - 1}\right)$. In (2.5), the first term is the optical carrier power after fiber transmission; the second term is the interaction between the two optical carriers; the third term is the power transfer as the result of Raman crosstalk between optical digital data and RF overlay channels. Note that if using (2.4), we cannot obtain an explicit expression of the third term as given in (2.5).

According to the definition of Raman crosstalk in [15], the electrical crosstalk suffered by the subcarrier in the RF overlay channel due to SRS is given by,

$$\text{Crosstalk (SRS)} \approx \left\{(\rho_{SRS}\,g_R P_N)^2\,\frac{1+e^{-2\alpha z} - 2e^{-\alpha z}\cos(2\pi f\Delta\tau\cdot z)}{\alpha^2 + (2\pi f\Delta\tau)^2}\right\} \qquad (2.6)$$

where ρ_{SRS} is the polarization overlap factor; g_R is the Raman gain coefficient; α is the attenuation coefficient of the fiber; f is the RF subcarrier frequency; $\Delta\tau$ is the group velocity mismatch between the two signals; z is the fiber length; and P_N is the normalized optical power of the optical digital data signal and can be expressed by the power spectrum density (PSD) [23], i.e.

$$P_N = P_{d0} \cdot \sqrt{G(f)} \tag{2.7}$$

where $G(f)$ is the PSD of optical digital data. The PSD is dependent on coding schemes and expressed with [24],

$$G(f) = \frac{4}{R_d} \cdot \left(\frac{\varepsilon - 1}{\varepsilon + 1}\right)^2 \frac{\sin^2\left(\frac{\pi f}{R_d}\right)}{\left(\frac{\pi f}{R_d}\right)^2} \quad \text{for NRZ} \tag{2.8}$$

$$G(f) = \frac{2}{R_d} \cdot \left(\frac{\varepsilon - 1}{\varepsilon + 1}\right)^2 \frac{\sin^2\left(\frac{\pi f}{2R_d}\right)}{\left(\frac{\pi f}{2R_d}\right)^2} \quad \text{for RZ} \tag{2.9}$$

$$G(f) = \frac{1}{R_d} \cdot \left(\frac{\varepsilon - 1}{\varepsilon + 1}\right)^2 \frac{\sin^2\left(\frac{\pi f}{2R_d}\right)}{\left(\frac{\pi f}{2R_d}\right)^2} \quad \text{for reverse RZ} \tag{2.10}$$

$$G(f) = \frac{4}{R_d} \cdot \left(\frac{\varepsilon - 1}{\varepsilon + 1}\right)^2 \frac{\sin^4\left(\frac{\pi f}{2R_d}\right)}{\left(\frac{\pi f}{2R_d}\right)^2} \quad \text{for Manchester} \tag{2.11}$$

where ε is the electrical extinction ratio of the digital data signal, f is the frequency, and

R_d is the data rate of the digital data channel.

In the case of SCM systems, CNR can be used to describe the system performance. The CNR is defined as the ratio of root mean square (RMS) power of subcarrier channel to RMS noise power of subcarrier channel at the receiver and can be expressed as,

$$\text{CNR} = \frac{\frac{1}{2}(m_{RF} R P_r)^2}{[i_{th}^2 + 2eRP_r + (RIN + Crosstalk(SRS))(RP_r)^2]B} \tag{2.12}$$

Here, at the numerator, it is RMS power per subcarrier channel. At the denominator, the first and second term is thermal noise and shot noise, respectively. RIN is the relative intensity noise of optical RF overlay channel transmitter. The Raman crosstalk generated at 1550 nm is given by (2.6). m_{RF} is the OMI of optical RF overlay channel, R is the detector responsivity of receiver, P_r is the average received optical power of RF overlay channel, and B is the effective noise bandwidth of each subcarrier channel at the receiver, which is 4.2 MHz for NTSC signals.

2.2 PON Systems under the Consideration

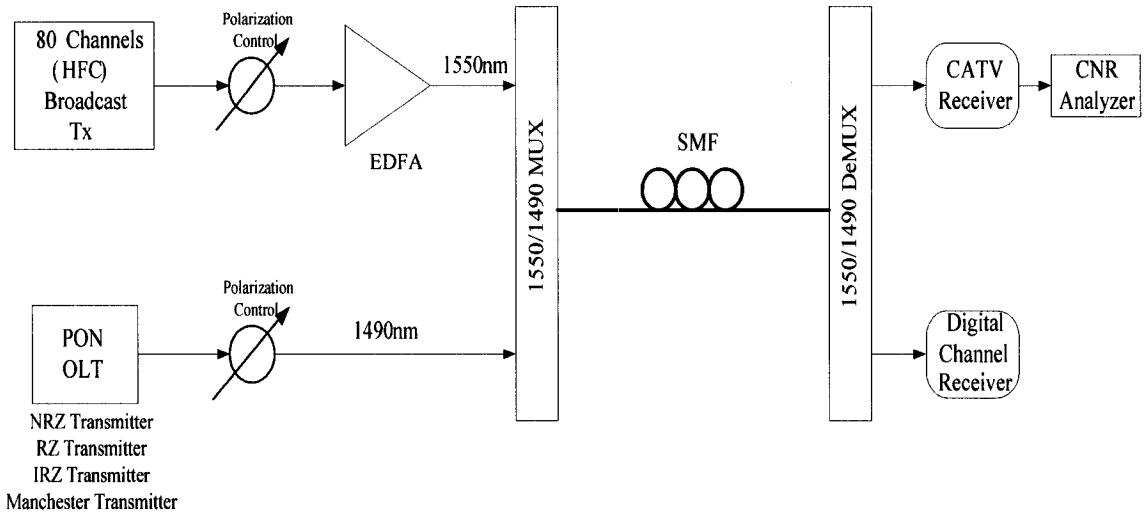

Fig. 2.2 - System architecture used for simulation

Fig. 2.2 illustrates the system setup that is used for our investigation. We consider a PON downstream system, which consists of an optical intensity modulated digital data channel at 1490 nm and an broadcast optical RF overlay channel at 1550 nm. The broadcast optical RF overlay channel carries 80 optical subcarriers, which are RF video subcarrier channels. The RF subcarrier frequency starts from 55.25 MHz (channel 2), and increases with 6 MHz frequency interval until 535.25 MHz. We use pseudorandom binary sequence (PRBS) of 2^{23}-1 with an additional "0" bit to model optical intensity modulation of the baseband digital data channel, and we do not consider time division multiplexing with idle frames used in PON systems.

The coding schemes of NRZ, RZ and inverse-RZ with 50% duty cycle and Manchester coding are considered in the baseband optical intensity modulation. Before

the broadcast optical RF overlay channel is launched into the fiber, an optical amplifier with noise free is used to have an input optical power of 17.7 dBm. Thus, without considering the impact of the optical digital data channel, the optical receiver of the broadcast optical RF overlay channel will be limited by thermal noise. The optical receiver has thermal noise of 7.5 $pA/\sqrt{Hz}$ and responsivity of 0.95 A/W. The optical intensity modulated digital data channel has data rate of 2.048 Gb/s, and has optical extinction ratio (ER) of 26 and 35 dB for NRZ, RZ and IRZ, and Manchester coding, respectively. A higher ER means a higher Raman crosstalk, and thus the Raman crosstalk is not underestimated. The fiber considered has loss of 0.22 dB/km at 1550 nm and 0.24 dB/km at 1490 nm, PMD of 0.1 $ps/\sqrt{km}$, effective Raman coefficient of 0.34 $1/(W \cdot km)$, and group velocity dispersion (GVD) induced walk-off of 0.96 ns/km between the two optical digital data and RF video overlay channels. The PMD correlation length of 50 meter is used to avoid underestimation of PMD influence.

The summary of system parameters is listed in Table 2.1. Because of 80 RF video subcarrier channels, we choose a channel which suffers from the worst Raman crosstalk, i.e. channel 2 at 55.25 MHz, to evaluate CNR in a bandwidth of 4.2 MHz. We use CNR degradation to evaluate the impact of Raman crosstalk and RIN transfer. The investigation is conducted in VPI Transmission Maker 7.01. Modeling of Raman amplification process in VPI Transmission Maker is obtained with coupled equations [25]. Insertion loss of all inline components is ignored, such as coarse WDM multiplexers.

Table 2.1 Summary of PON system parameters

Optical digital data channel	Optical RF overlay channel	Transmission fiber
Wavelength: 1490 nm	Wavelength: 1550 nm	PMD: 0.1 $ps/\sqrt{km}$
Optical power(P_d): 2 dBm	Optical power(P_{RF}): 17.7 dBm	GVD walk-off($\Delta\tau$): 0.96 ns/km
Optical ER(ε): 26 dB for NRZ and RZ, and 35 dB for IRZ and Manchester	RF overlay: 80 RF video channels Starting from 55.25 MHz, Every 6 MHz	Fiber loss(α): 0.24 dB/km at 1490 nm and 0.22 dB/km at 1550 nm
RIN: -160 dB/Hz	RIN: -165 dB/Hz	Effective Raman coefficient(g_R): 0.34 $1/(W \cdot km)$
*Data rate(R_d): 2048 Mb/s	OMI: 3.5%	PMD correlation length: 50 m

*For NTSC analog simulation, we use a resolution of 0.125 MHz because video subcarrier frequency of NTSC channels, which is 55.25, 61.25, and 67.25 MHz etc., can be divided exactly by 0.125MHz. In the simulation, if we need a resolution of 0.125 MHz, the time window of simulation should be reciprocal of the resolution, i.e. 8×10^{-6} second. Because the time window multiples bite rate must be 2^n in the simulation, we set data rate of 2.048Gb/s instead of 2.488Gb/s. However, this assumption does not alter the evaluation of Raman crosstalk.

2.3 Modules Used for Simulation

2.3.1 Power Budget

One constraint on the video system is Stimulated Brillion Scattering (SBS) limit. Stimulated Brillouin scattering arises from the fact that a strong optical signal propagating in a fiber generates an acoustic wave that produces variations in the refractive index. These index variations cause lightwaves to scatter in the backward direction toward the transmitter. When the power is low, the effect of SBS is negligible.

Shown in Fig. 2.3, if the input power levels are greater than a certain signal level threshold (horizontal dash line), the backscattered power (line) because of SBS will increase steeply. After the input power (dash line) reaches the SBS limit, the additional optical power will merely is scattered backward. As a result, the effect of SBS can increase nonlinear noise at the receiver, and degrade CNR.

Because standard G.652 single-mode fiber has an SBS limit of 16 to 20dBm, the input analog video signal power is set to 17.7 dBm in our investigation [26].

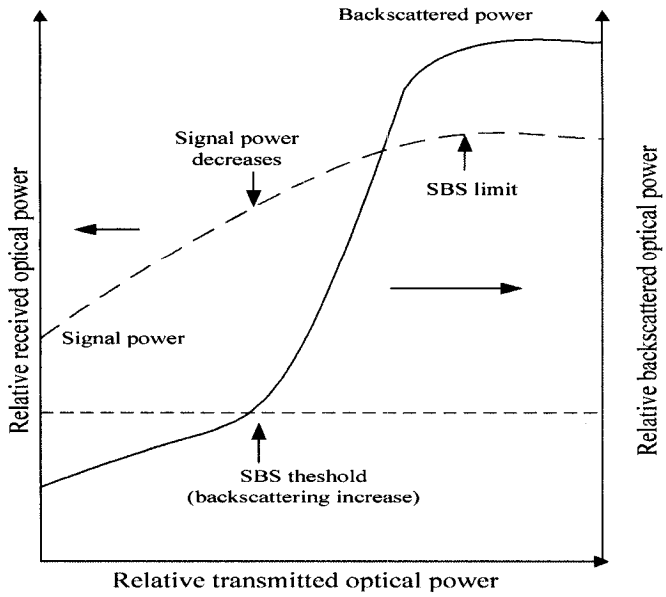

Fig. 2.3 - Effect of SBS on signal power in an optical fiber

Power level of the data channel which is transmitted from the OLT at 1490 nm will cause SRS induced noise to the 1550nm RF overlay signal. Optical power level for the downstream digital data channel can be set from 1.5 to 5 dBm. In our investigation we set the optical power from 0 to 4 dBm for the optical digital data channel.

2.3.2 Optical Source for PON

In the simulation, we use directly modulated laser as the CATV analog channel optical source. This module models a laser which is driven with 80 NTSC video carrier signals.

In the simulation, we use parameters to describe the laser including RIN (at a specified power), linewidth, driver transconductance, laser bias, and so on. The general 1550-nm laser parameters that are used in the simulation are shown in Table 2.2,

Table 2.2 General parameters of 1550nm laser

Name and Description	Unit	Default Value
Emitting Frequency	THz	193.4
RIN	dB/Hz	-165.0
Linewidth	MHz	10.0
Threshold Current	mA	20
Driver Transconductance	A/V	1.0/50.0
Laser Bias	mA	100

Also, we use an external modulated CW laser as the optical digital data channel optical source. Its parameters are shown in Table 2.3, including RIN (at a specified power), and linewidth.

Table 2.3 General parameters of 1490nm laser

Name and Description	Unit	Default Value
Emission Frequency	THz	201.2
RIN	dB/Hz	-170.0,-160.0,-150.0,-140.0,-130.0,-120
Linewidth	MHz	10.0

2.3.3 Modulation Index of Optical RF Overlay Channel

In general, the signal current at each subcarrier channel is fully dependent upon the optical modulation index (OMI), "m_{RF}", which is a measure of the ratio of the peak modulation of the individual video subcarrier channel to the average optical power of RF

overlay channel.

For a SCM system with 80 subcarrier channels, the maximum OMI for each channel is 1/80, i.e. 1.25%. In common CATV systems, the OMI is twice or more of the reciprocal of the channel number, i.e., summation of all the modulation indexes will give over 100% modulation. In the practice, the individual channels are not modulated coherently, and the signals add up statistically. As a consequence, the sum of all the modulation indexes will not reach 100%, and the laser is operated in the linear region [27].

In this thesis, the CATV system, which is composed of 80 video subcarrier channels, should have OMI in the range of 3.5% to 5.0% in order to meet 48 dB or higher CNR. When OMI is higher than 5.0%, clipping noise becomes dominant. Therefore, we only consider the CNR degradation in the OMI range from 3.0% to 4.5%.

Shown in Fig. 2.4, the total injection current of analog CATV direct modulated laser J(t) consists of the bias current J_{bias}, the modulation current $J_{\mathrm{mod}}(t)$, and the laser threshold current J_{th}.

According the definition of OMI, we can get optical modulation index "m_{RF}" of direct modulation laser from Fig. 2.4,

$$m_{RF} = \left(\frac{I_m}{I_{bias} - I_{th}} \right) = \frac{I_m}{I_{th}} \left(\frac{1}{\frac{I_{bias}}{I_{th}} - 1} \right) \tag{2.13}$$

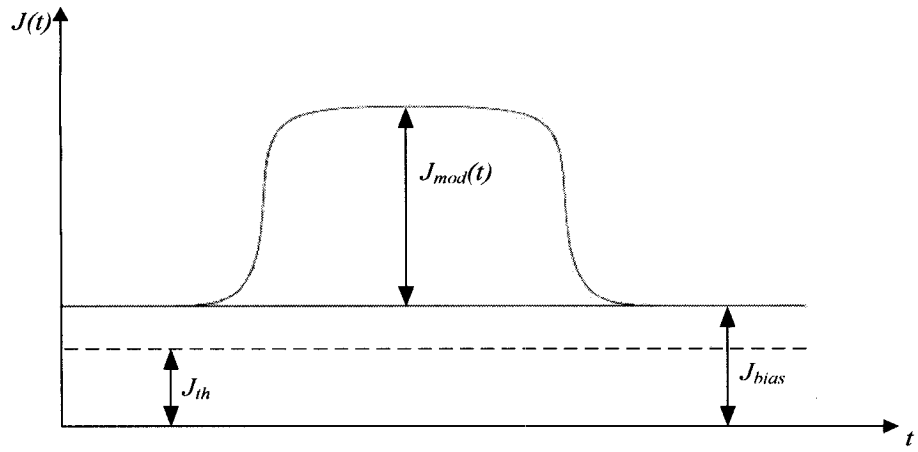

Fig. 2.4 - Injection current of RF directly modulated laser.

In the simulation, modulation current I_m can be calculated from equation,

$$I_m = (A_{channel} \times T_{laser}) \tag{2.14}$$

where $A_{channel}$ is signal amplitude per channel and T_{laser} is driver transconductance of laser.

From Table 2.2, driver transconductance is 1/50 A/V, laser bias I_{bias} is 100mA and laser threshold current I_{th} is 20m, so $\frac{I_m}{I_{th}}$ equals to $A_{channel}$ and $\frac{I_{bias}}{I_{th}}$ equals to 5.

As a result, OMI of CATV direct modulation laser in the simulation can be determined by

$$m_{RF} = \frac{A_{channel}}{4} \tag{2.15}$$

2.3.4 Fiber for PON Systems

According to Table 2.4, we set our simulation fiber module parameter according to

Corning single mode fiber (SMF) that is fully in compliant with ITU-T G.652 standards for single-mode optical fiber.

Table 2.4 Fiber parameters

Fiber Type and Trade Name	Attenuation at 1490nm(1550nm) (dB/km)	A_{eff} (um^2)	D(C band) [ps/(km-nm)]	Slope S [ps/(km-nm^2)]	PMD ($ps/\sqrt{km}$)
SMF	0.24 (0.22)	80	17	0.09	0.1

Fig. 2.5 shows the optical loss spectrum of conventional single-mode fiber that is used in the simulation.

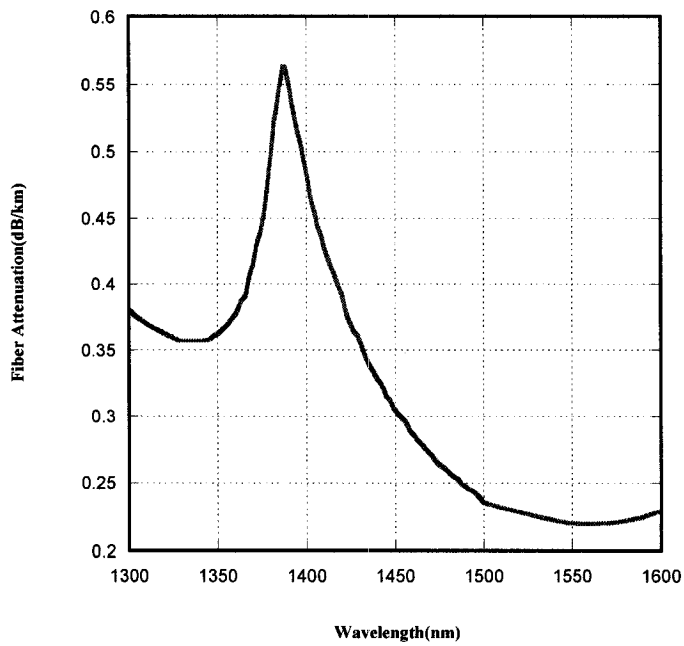

Fig. 2.5 - Optical loss spectrum of conventional single-mode fiber.

2.3.5 Data Coding Schemes

Recent analysis [19] has demonstrated the Raman effect can be mitigated by spectrum control of the data idle pattern. During the 67% controllable time, the idle patterns can be designed to shift the digital signal's spectral density to regions that are less injurious to the PON video overlay. Such improvement could eliminate the need for low channel pre-emphasis that is commonly used today.

For a long time, NRZ has been the dominant modulation format in IM/DD fiber-optical communication systems. Fig. 2.6 shows the block diagram of transmitter and optical signal spectrum of NRZ. In general, NRZ modulated optical signal has the most compact spectrum compared to that with other modulate formats.

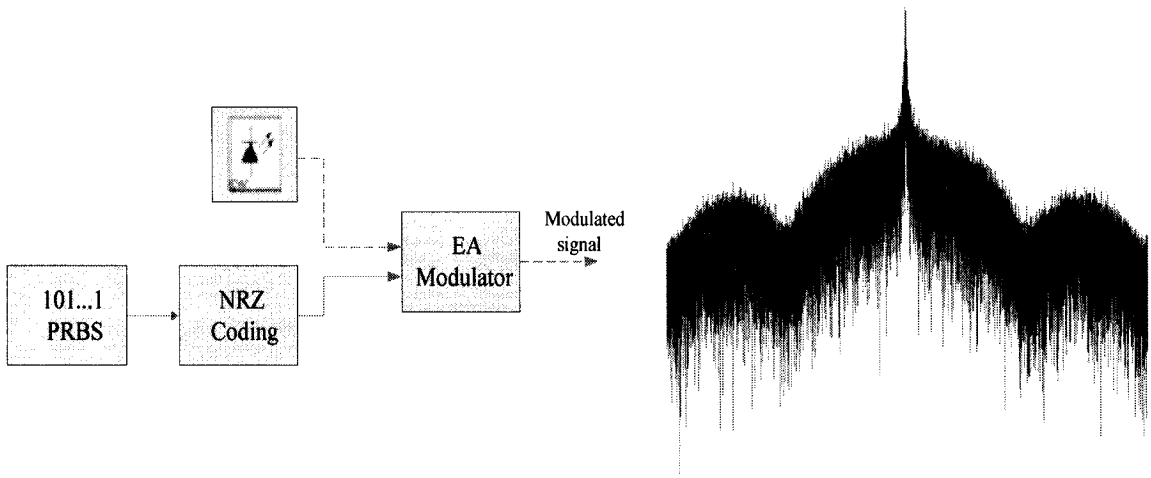

Fig. 2.6 - Block diagrams of transmitter and signal spectrum of NRZ.

Fig. 2.7 shows the block diagram of transmitter and optical signal spectrum of RZ with 50% duty cycle. RZ optical signal has been found to be more tolerant to nonlinearity than NRZ optical signal. Compared to NRZ, it has a wider spectrum because of its

narrower pulse width.

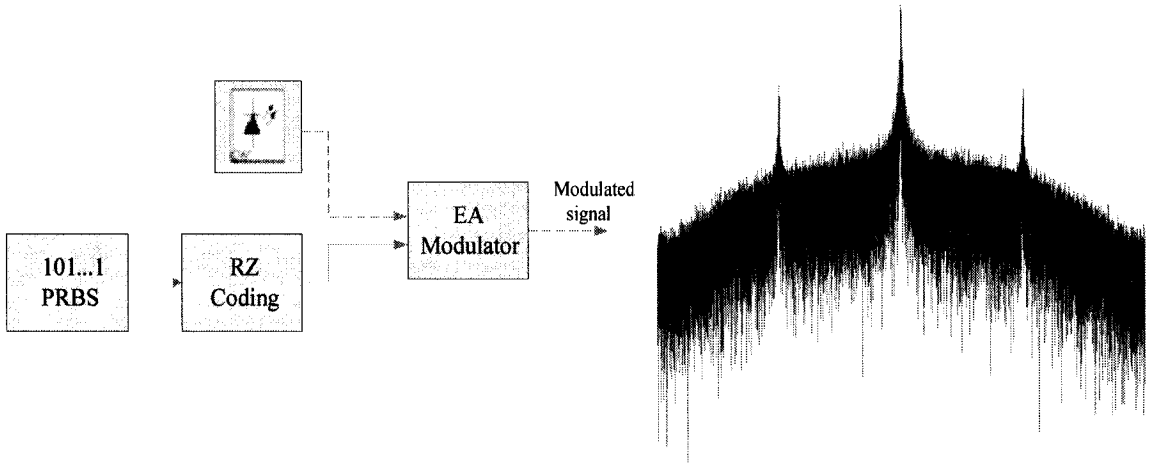

Fig. 2.7 - Block diagrams of transmitter and signal spectrum of RZ.

Fig. 2.8 shows the block diagram of transmitter and optical signal spectrum of IRZ. An IRZ signal is generated by inverting the intensity level of a conventional RZ signal with 50% duty cycle by a MZ-IM at the quadrature point of the negative slope of transmission curve. A downstream IRZ signal has been proposed to use for wavelength reuse for the upstream link in a WDM PON [22].

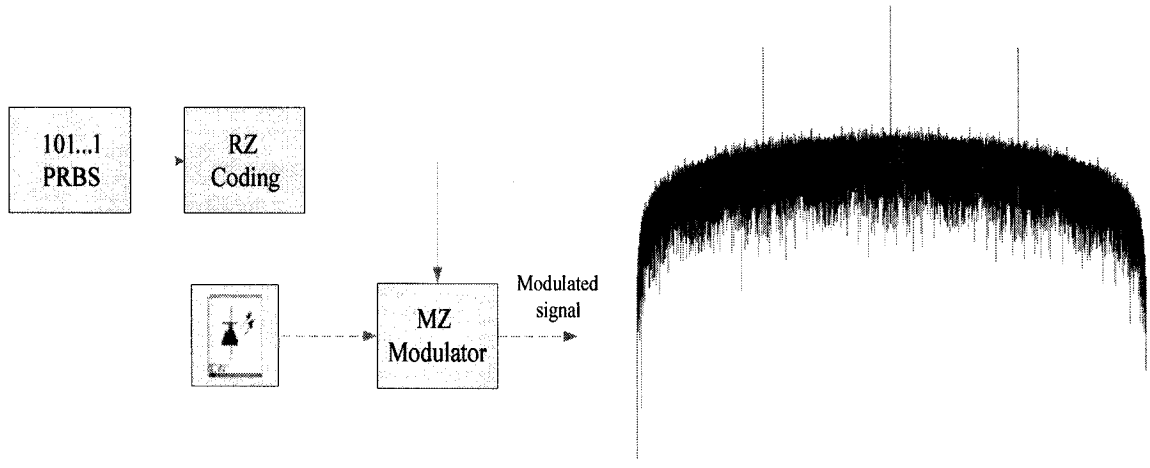

Fig. 2.8 - Block diagrams of transmitter and signal spectrum of IRZ.

Fig. 2.9 shows the block diagram of transmitter and optical signal spectrum of Manchester. Compared to NRZ and RZ, it has no DC component and is easy to recover clock.

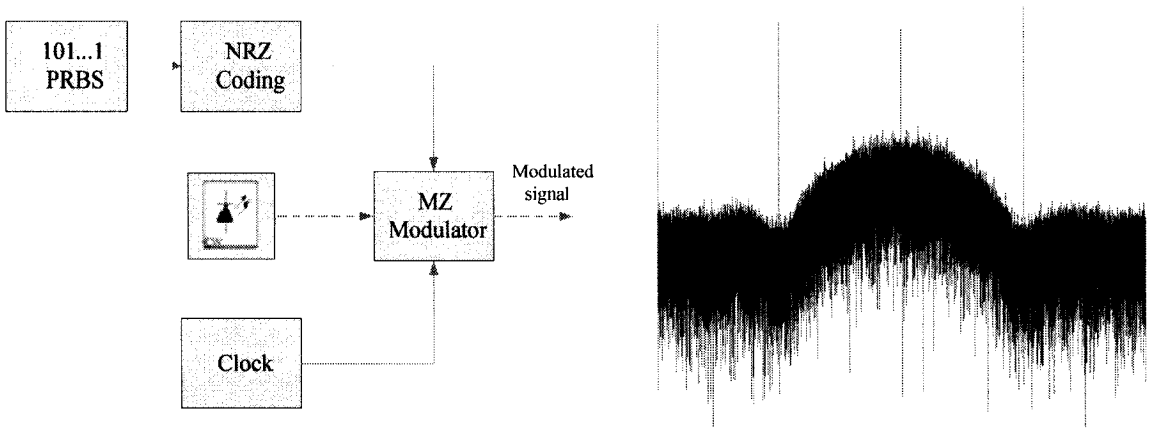

Fig. 2.9 - Block diagrams of transmitter and signal spectrum of Manchester.

Fig. 2.10 shows the power spectrums density of NRZ, RZ, IRZ, and Manchester coding schemes derived from (2.8) to (2.11). Based on (2.7), we know that Raman crosstalk is dependent on the signal power spectrums density of the digital data channel. From Fig. 2.10 we find that IRZ has lower power density at the low frequency than RZ or NRZ, so Raman effect of IRZ on RF video subcarrier channels is expected to be better than NRZ and RZ. Particularly, Manchester coding has a spectrum that is centered on half the bit-rate and has no DC component. As a result, Manchester should have little Raman crosstalk on low frequency of RF video subcarrier channels in PON.

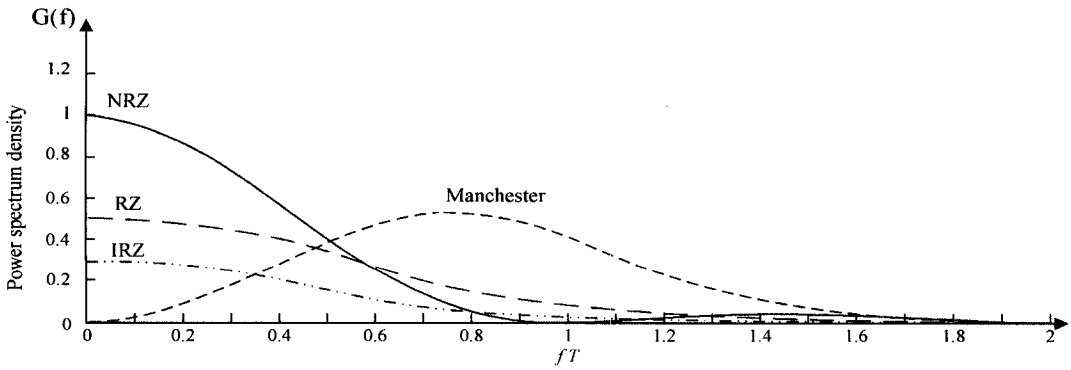

Fig. 2.10 - Power spectrum density of NRZ, RZ, IRZ, and Manchester coding schemes.

CHAPTER 3 NUMERICAL ANALYSIS AND DISCUSSIONS

In this chapter, we evaluated Raman crosstalk induced CNR degradations in RF overlay channel of PON systems considering four coding schemes: NRZ, RZ, IRZ, and Manchester. Section 3.1 presents the spectral characteristic of Raman Crosstalk in RF overlay channel. Section 3.2 shows the investigation of Raman crosstalk induced CNR degradation with a virtual assumption that fiber has no PMD when polarization states of optical video overlay and digital channels maintain in parallel or orthogonal aligned along the fiber. Section 3.3 illustrates Raman crosstalk with the consideration of PMD, i.e. real fiber. For this case, we investigate CNR degradation due to Raman crosstalk if polarization states along a fiber have random evolution due to PMD. Thus, we can evaluate the PMD impact on Raman crosstalk induced CNR degradation. Finally, we evaluate RIN transfer impact on CNR in Section 3.4

In the evaluation of degradation, for the optical RF overlay channel we set up a reference CNR without Raman crosstalk using parameters in Table 3.1,

Table 3.1 Reference parameters without Raman Crosstalk

RIN OVERLAY (dB/Hz)	-165
OMI	3.5%

3.1 Spectral characteristic of Raman crosstalk in PON systems

In general, Raman crosstalk has the worst impact on the lowest frequency video channels [17]. Fig. 3.1 shows the simulation result of Raman crosstalk degradation in a

function of RF video subcarrier frequency for parallel-aligned polarization states at the fiber input with and without PMD. Because of the walk-off of the two signal channels at 1490 nm and 1550 nm due to fiber dispersion, Raman Crosstalk effect has low-pass characteristic, and makes the Raman impact on the lower frequency channels more serious than the higher frequency channels.

With the consideration of the impact of PMD, the instantaneous transfer functions vary with time, but the maximum-hold values are deterministic and has similar low-pass characteristic [10]. For NTSC video system, the CNR degradation is the greatest at the lowest frequency channels. Channel 2 at 55.25 MHz has the worst CNR degradation because of Raman crosstalk. As a result, in the following evaluations, we used Channel 2 at 55.25 MHz to evaluate the CNR degradation due to Raman crosstalk.

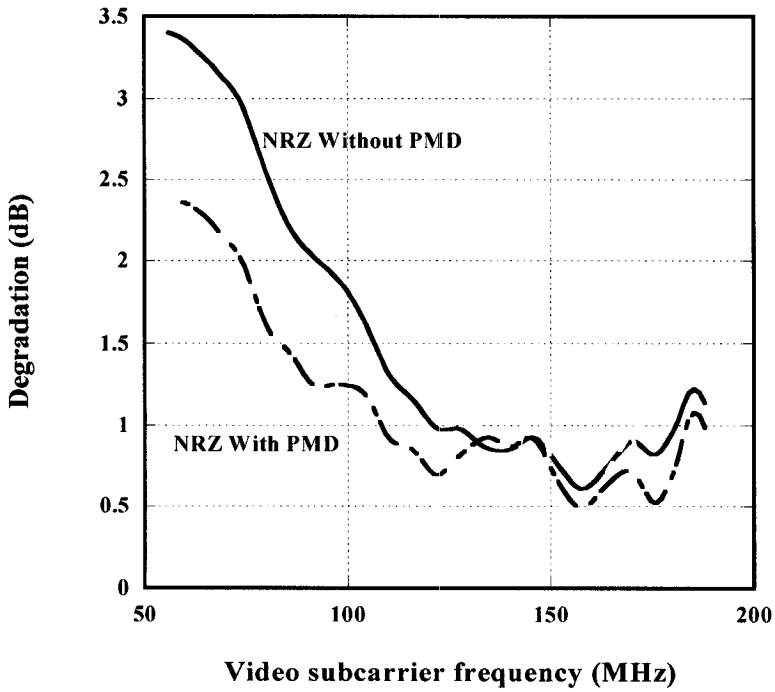

Fig. 3.1 - Raman crosstalk induced CNR degradation as a function of channel frequency

in an 8.5 km fiber system for the modulation format of NRZ. The two optical channels at 1490 nm and 1550 nm have parallel aligned polarization states at the fiber input. The other parameters are given in Table 2.1

3.2 Raman crosstalk induced CNR degradation: the worst and best cases

When PMD impact is not considered, the same polarization states maintain along the fiber as setting at fiber input. Thus, parallel-aligned polarization states between the two optical channels result in highest Raman crosstalk, i.e. the worst case. On the contrary, the lowest Raman crosstalk can be obtained if orthogonal-aligned polarization states along a fiber are set, i.e. the best case. Consequently, we obtain the upper and lower limits of CNR degradation induced by Raman crosstalk.

3.2.1 Raman crosstalk induced CNR degradation as a function of fiber length

In this part, we measure the CNR degradation caused by Raman Crosstalk at CATV Channel 2 (55.25MHz) as a function of fiber length.

Fig. 3.2 and Fig. 3.3 show Raman crosstalk induced CNR degradation as a function of fiber length for parallel-aligned and orthogonal-aligned polarization states between the two optical channels, respectively. The CNR degradation is defined a ratio of CNR between two PON systems in which the 1490-nm optical digital data channel is turned "on" and "off" in optical power. Thus, when the 1490-nm channel is turned "off", the 1550-nm RF overlay channel does not experience Raman crosstalk, and otherwise the

1550-nm RF overlay channel does.

Fig. 3.2 shows that modulation schemes of NRZ, RZ, and IRZ strongly depend on fiber length in Raman crosstalk and the worst Raman crosstalk occurs at 8.5 km, which is very close to theoretical prediction [15-18, 24]. The RZ format results in a ~1.4dB lower Raman crosstalk compared to NRZ at 8.5 km. This is due to the fact that high optical power level in bit "1" in RZ is shorter in time duration than that in NRZ and the RZ' power density at the lower frequency is only half of the NRZ's. Furthermore, the IRZ format results in a ~1.3dB lower Raman crosstalk compared to RZ at 8.5 km. This is due to the fact that the IRZ' power density at the lower frequency is only half of the RZ's.

However, for Manchester coding format, Raman crosstalk induced CNR degradation is very small, less than 0.3 dB, even though parallel-aligned polarization states along the whole of fiber are assumed. This verifies that shaping the optical spectrum of the 1490-nm optical digital data channel using Manchester coding can reduce Raman crosstalk. This is because Manchester coding results in high frequency centered power spectrum density, and thus the Raman crosstalk at the lower frequencies is very low [19].

CNR degradation shown in Fig. 3.2 is the worst case for this considered PON system.

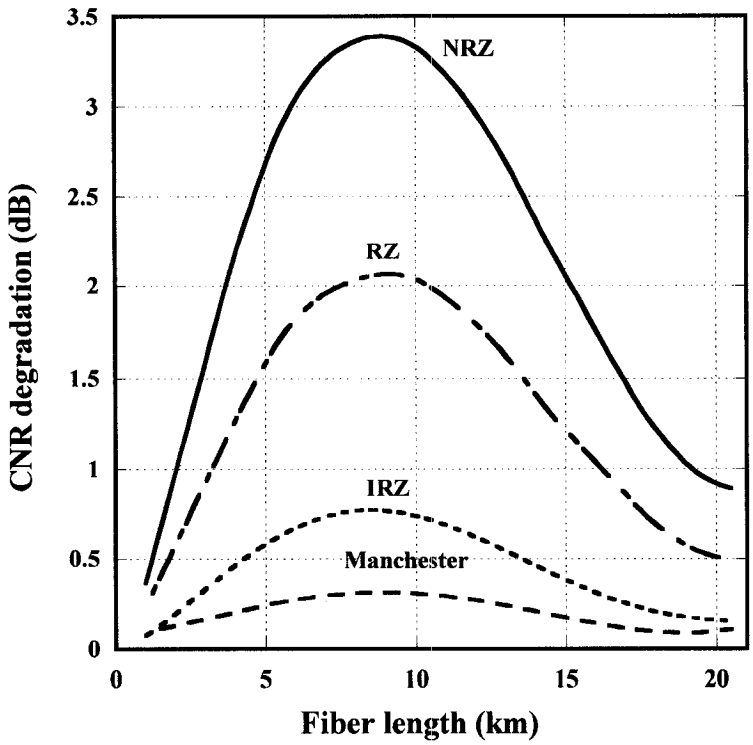

Fig. 3.2 - Raman crosstalk induced CNR degradation as a function of fiber length for modulation formats of NRZ, RZ, IRZ, and Manchester. The fiber is assumed no PMD. The two optical channels at 1490 nm and 1550 nm have parallel-aligned polarization states at fiber input. The other parameters are given in Table 2.1

Corresponding to Fig. 3.2, Fig. 3.3 shows that Raman crosstalk hardly occurs if orthogonal-aligned polarization states of the two optical channels along the whole of fiber never be altered. This is because Raman gain for a signal polarization state orthogonal to the pump is less than one tenth that parallel [15, 25]. Therefore, this is the lowest Raman crosstalk induced CNR degradation for this considered PON system, i.e. the best case.

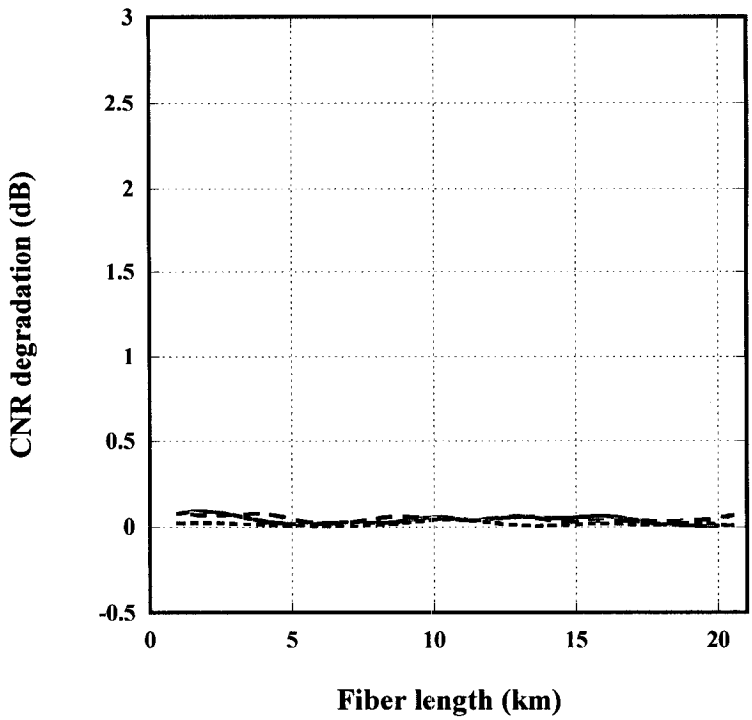

Fig. 3.3 - Raman crosstalk induced CNR degradation as a function of fiber length for modulation formats of NRZ, RZ, IRZ, and Manchester. The fiber is assumed no PMD. The two optical channels at 1490 nm and 1550 nm have orthogonal-aligned polarization states at fiber input. The other parameters are given in Table 2.1

3.2.2 Raman crosstalk induced CNR degradation as a function of optical power of optical digital data channel

In Fig. 3.2 and Fig. 3.3, we only consider 2-dBm optical power of the 1490-nm optical digital data channel, which is the pump for the Raman crosstalk. To obtain the impact of optical power of the 1490-nm optical digital data channel on CNR degradation, we investigate CNR degradation as a function of optical power of the 1490-nm optical digital data channel at the worst fiber length of 8.5 km. Fig. 3.4 shows CNR degradation

for the case of parallel-aligned polarization states between the two optical channels. As shown in Fig. 3.4, with the increase of optical power of the 1490-nm optical digital data channel, CNR degradation increases significantly for NRZ and RZ, but for IRZ and Manchester coding the increase is very gradual. At 3-dBm optical power of the 1490-nm optical digital data channel, simulated CNR degradation is ~4.6 dB for NRZ, very close to the measured [17].

That means Raman crosstalk induced by IRZ and Manchester coding is not sensitive to the optical digital data power.

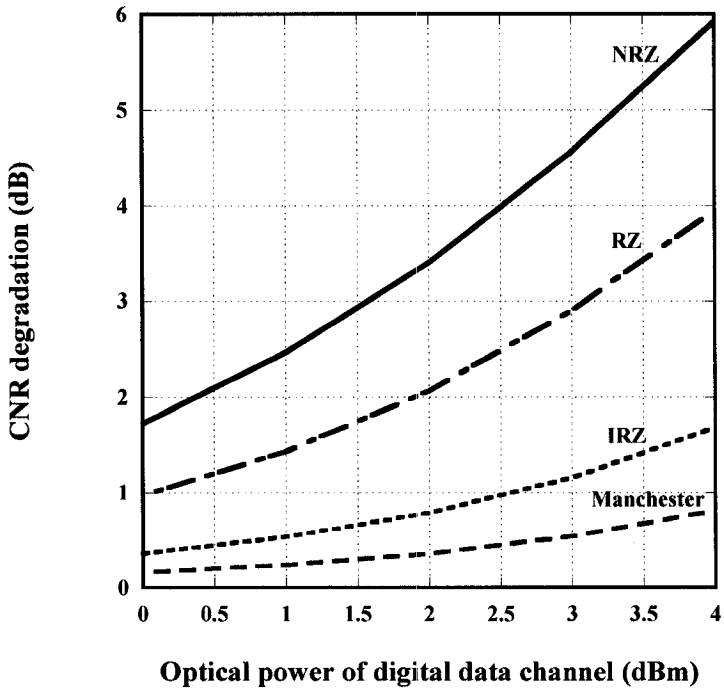

Fig. 3.4 - Raman crosstalk induced CNR degradation as a function of optical power of digital data channel. The two optical channels at 1490 nm and 1550 nm have parallel-aligned polarization states at fiber input. The fiber is assumed no PMD with fiber length of 8.5 km. The others are given in Table 2.1.

When orthogonal-aligned polarizations states maintain along the fiber, Raman crosstalk induced CNR degradation is negligibly small and is shown in Fig. 3.5.

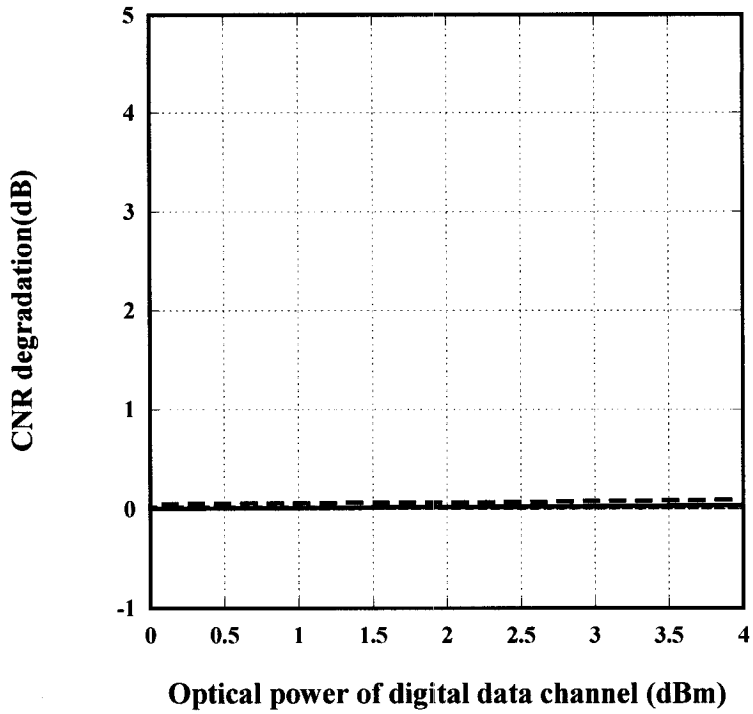

Fig. 3.5 - Raman crosstalk induced CNR degradation as a function of optical power of digital data channel. The two optical channels at 1490 nm and 1550 nm have orthogonal-aligned polarization states at fiber input. The fiber is assumed no PMD with fiber length of 8.5 km. The others are given in Table 2.1

3.2.3 Raman crosstalk induced CNR degradation as a function of optical modulation index of CATV channel

To reduce the impact of Raman crosstalk, a technique is to use pre-emphasized RF power in RF overlay channels. But the maximum optical modulation index is limited by modulation dynamics of the laser and nonlinear distortion due to optical subcarrier

modulation. From Fig. 3.6, we find when modulation index is over 4.5%, clipping noise will increase dramatically and make CNR decrease steeply.

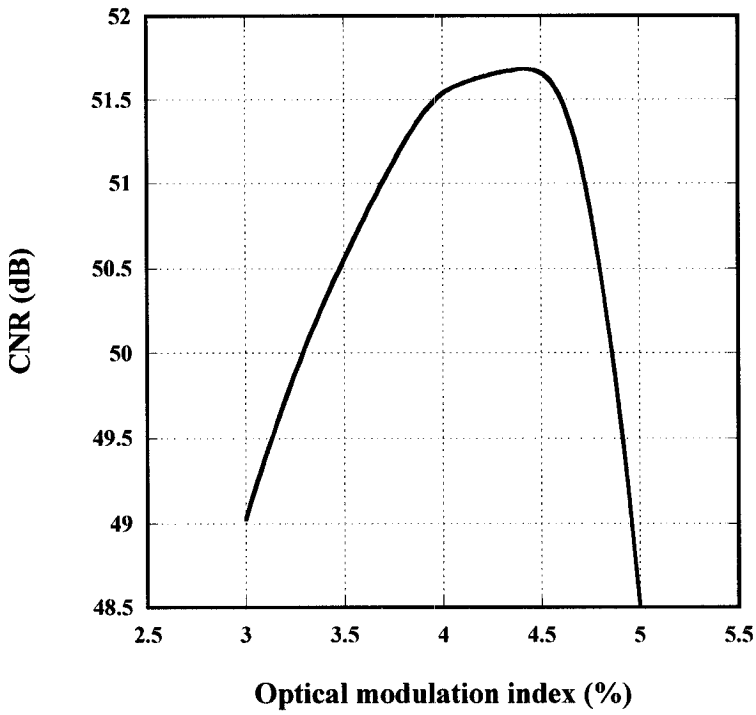

Fig. 3.6 - CNR of CATV channel without Raman crosstalk as a function of modulation index. The fiber is assumed no PMD with fiber length of 8.5 km. The digital data channel is not considered.

The effectiveness of this technique is investigated and shown in Fig. 3.7 and Fig. 3.8 for RF channel 2. In Fig. 3.7, we consider the worst case: parallel-aligned polarization states between the two optical channels. Fig. 3.7 shows that CNR degradation decreases gradually with increase of optical modulation index in the range of 3% to 4.5% as expected. Therefore, it is found that the increase of optical modulation index from 3% to 4.5% only leads to relatively a small decrease of CNR degradation induced by Raman

crosstalk for NRZ, RZ, and IRZ if the fiber has no PMD, i.e. parallel polarization states maintained along the fiber. For Manchester coding the CNR degradations are below 0.5 dB, so the optical modulation index increasing has little effect on the CNR degradation.

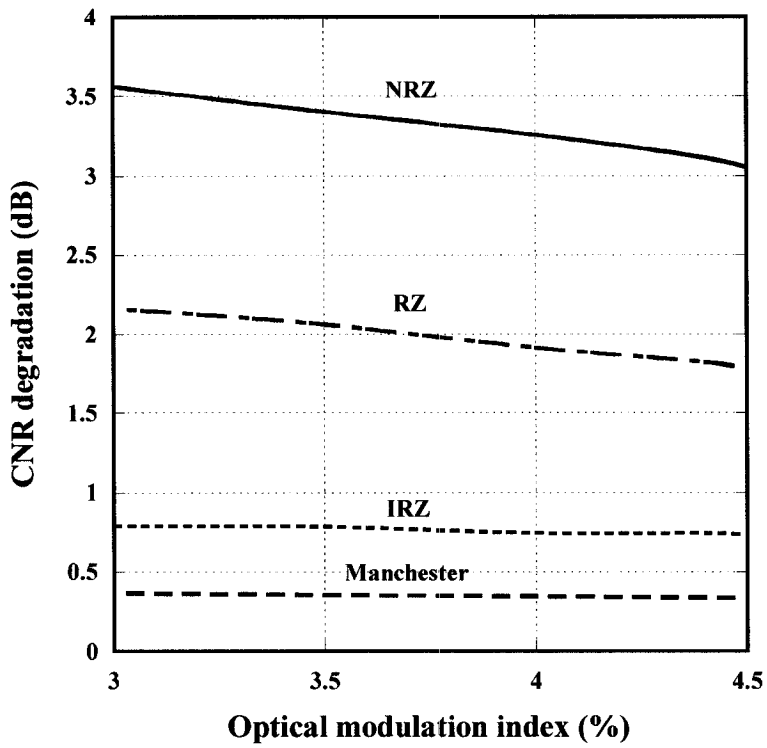

Fig. 3.7 - CNR degradation due to Raman crosstalk as a function of optical modulation index of optical RF overlay channel for the case of parallel-aligned polarization states between the two optical channels. The fiber is assumed no PMD with fiber length of 8.5 km. and the others are the same as in Table. 2.1.

When orthogonal-aligned polarizations states maintain along the fiber, Raman crosstalk induced CNR degradation is negligibly small and is shown in Fig. 3.8.

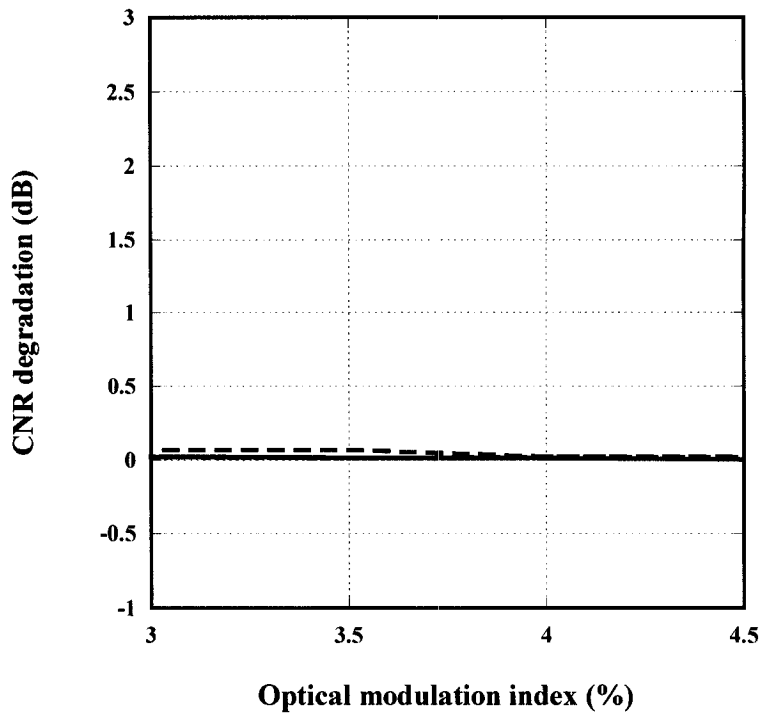

Fig. 3.8 - CNR degradation due to Raman crosstalk as a function of optical modulation index of optical RF overlay channel for the case of orthogonal-aligned polarization states between the two optical channels. The fiber is assumed no PMD with fiber length of 8.5 km. and the others are the same as in Table. 2.1.

3.3 Raman crosstalk induced CNR degradation: impact of fiber PMD

In Section 3.2, we ignore the Polarization Mode Dispersion (PMD) effect which will make the two polarized signals-1490nm digital channel and 1550 video channel walk-off each other. Without loss of generality, we consider a fiber with PMD of 0.1 $ps/\sqrt{km}$ in this section.

PMD has a random nature because of birefringence varies along the fiber randomly. The analytical treatment of PMD is quite complex in general because of its statistical

nature. In the simulation, we take the statistical results of each data and iterate the simulation until an almost stable CNR is obtained.

3.3.1 Raman crosstalk induced CNR degradation as a function of fiber length

It is seen that CNR degradation as shown in Fig. 3.9 is reduced by ~1.1 and 0.7 dB at 8.5 km for NRZ and RZ, respectively, compared to Fig. 3.2. This is because polarization states along the fiber do not always maintain parallel due to PMD, and thus Raman crosstalk is reduced correspondingly [11].

However, for IRZ and Manchester coding, PMD does not have a visible impact on CNR, which is obvious by comparing Fig. 3.2 and Fig. 3.9. This is due to the fact that Raman crosstalk induced CNR degradation is negligibly small in IRZ and Manchester coding even for the worst case, and thus PMD of course has no impact on CNR.

Moreover, with the increase of fiber length, e.g. 20 km, it is found that PMD does not obviously reduce Raman crosstalk by comparing Fig. 3.2 and Fig. 3.9 for NRZ and RZ, about 0.2 and 0.05 dB CNR degradation reduction due to PMD for NRZ and RZ at 20 km, respectively. In fact, it is impossible for such a small PMD induced CNR changes to be seen experimentally.

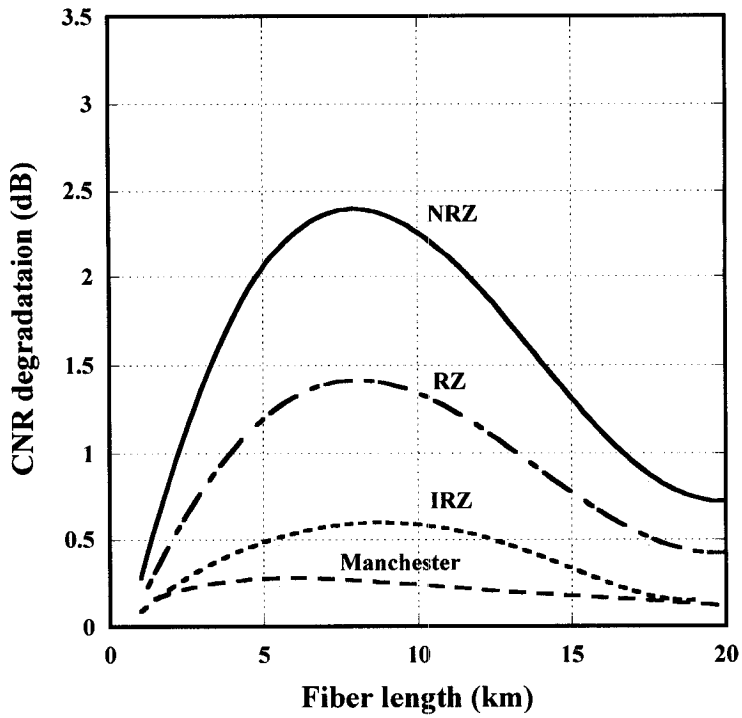

Fig. 3.9 - Raman crosstalk induced CNR degradation as a function of fiber length for parallel-aligned polarization states at the fiber input. The fiber PMD of 0.1 $ps/\sqrt{km}$, and correlation length of 50 m were used in simulation, and the others are the same as in Table 2.1

When orthogonal-aligned polarization states between the two optical channels at the fiber input are set, CNR degradation as shown in Fig. 3.10 is increased for NRZ, RZ, IRZ, and Manchester, particularly for NRZ and RZ, compared to Fig. 3.3 in which fiber PMD is not included, i.e. the best case. This is because the orthogonal polarization states no longer maintain along the fiber even though the polarization states at the fiber input are set orthogonal.

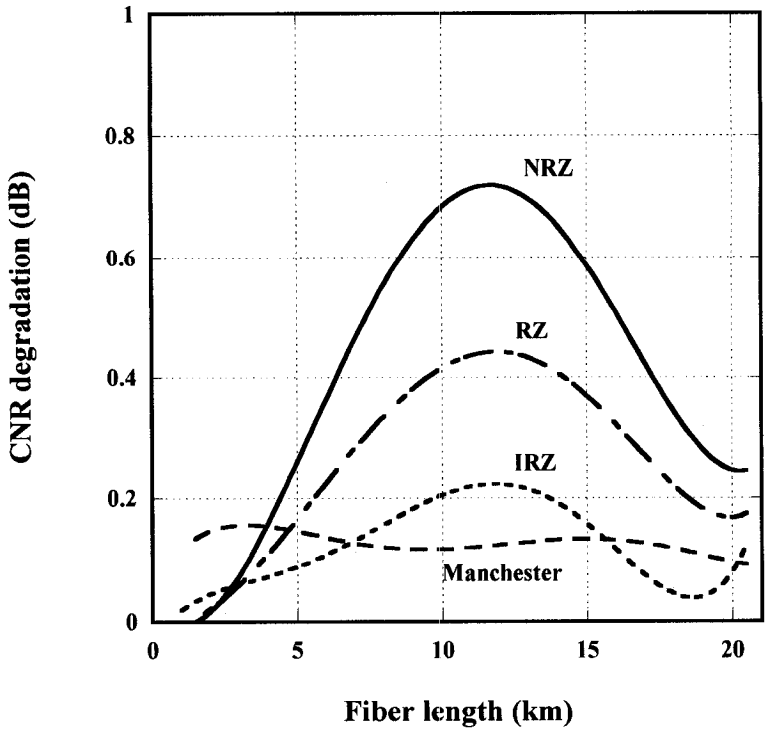

Fig. 3.10 - Raman crosstalk induced CNR degradation as a function of fiber length for orthogonal-aligned polarization states at the fiber input. The fiber PMD of 0.1 $ps/\sqrt{km}$, and correlation length of 50 m were used in simulation, and the others are the same as in Table 2.1

However, by comparing Fig. 3.9 and Fig. 3.10, it is clearly shown that the orthogonal-aligned polarization states at the fiber input are still helpful for all NRZ, RZ, IRZ, and Manchester, particularly for NRZ and RZ, in the reduction of Raman crosstalk. If fiber length is less than 15 km the reduction of Raman crosstalk using orthogonal polarization states at the fiber input is obvious. However, at fiber length of 20 km, the reduction of Raman crosstalk is small, about 0.5 dB for NRZ. The reason of Raman crosstalk reduction due to orthogonal polarization states is given as follows. The Raman

crosstalk along the fiber is accumulated processing. Given the fact that optical power of the 1490-nm optical digital data channel is highest at the fiber input, which will induce a biggest Raman crosstalk, the Raman crosstalk will be reduced if orthogonal polarization states are set in the fiber input. Also, the biggest Raman crosstalk occurs at around 8.5 km, i.e. the worst Raman crosstalk length. The occurring probability of parallel-aligned polarization states around fiber length of 8.5 km may be reduced when orthogonal-aligned polarization states at the fiber input are set even though PMD manipulates the polarization states along the fiber. This is dependent on PMD value and PMD correlation length. If the Raman crosstalk around fiber length of 8.5 km is reduced, the accumulated Raman crosstalk for fiber length of more than 8.5 km may be reduced. Therefore, our results show that orthogonal polarization state setting is still helpful to reduce Raman crosstalk to some extent if fiber length is less than 15 km.

In order to clearly show the reduction of Raman crosstalk impact using the orthogonal polarization state setting at the fiber input, we compare Fig. 3.9 with Fig. 3.10 and obtain CNR degradation reduction by using orthogonal-aligned polarization state setting at the fiber input, as shown in Fig. 3.11. It is found that orthogonal-aligned polarization state setting at the fiber input results in a reduction of ~1.9 and ~1.1 dB CNR degradation at the fiber length of 8.5 km for NRZ and RZ, respectively. However, at the fiber length of 20 km, the reduction becomes very small, less than 0.5 dB.

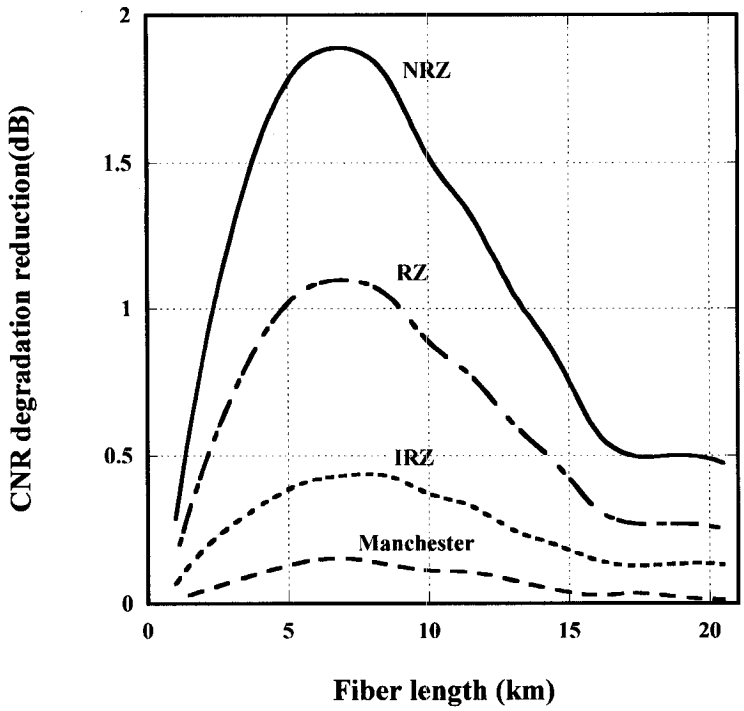

Fig. 3.11 - CNR degradation reduction due to using orthogonal-aligned polarization states compared to parallel-aligned polarization states at the fiber input with fiber PMD of 0.1 $ps/\sqrt{km}$. The others are the same as in Table 2.1.

3.3.2 Raman crosstalk induced CNR degradation as a function of optical power of optical digital data channel

Corresponding to Fig. 3.4 and Fig. 3.5, Fig. 3.12 and Fig. 3.13 show CNR degradation versus optical power of the optical digital data channel for a fiber length of 8.5 km, in which fiber PMD of 0.1 $ps/\sqrt{km}$ is considered. For both cases of parallel-aligned and orthogonal-aligned polarization states at the fiber input, CNR degradation increases with optical power of the optical digital data channel, particularly for NRZ and RZ.

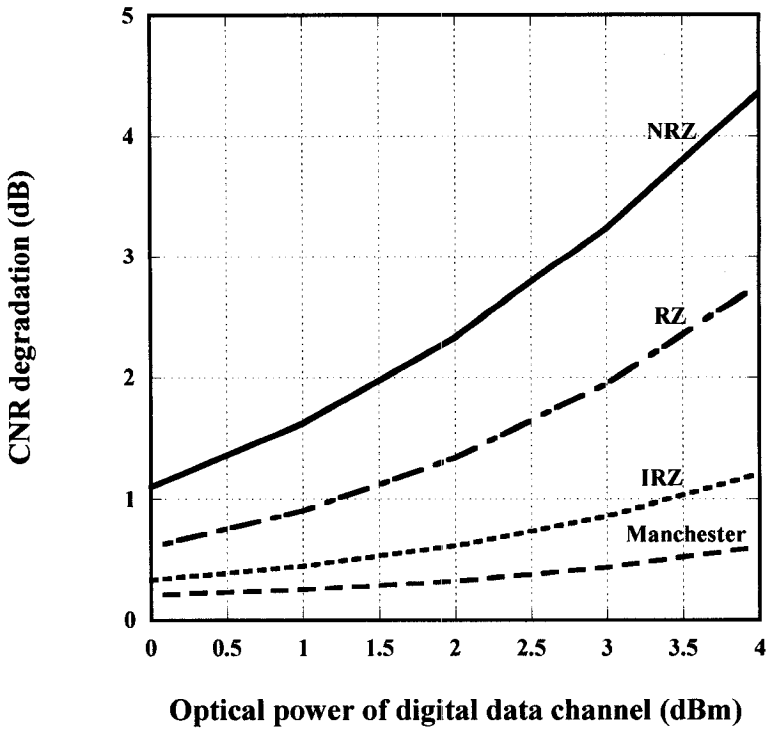

Fig. 3.12 - Raman crosstalk induced CNR degradation as a function of optical power of the digital data channel for parallel-aligned polarization states at the fiber input. The fiber length is 8.5 km with PMD of 0.1 $ps/\sqrt{km}$, and the others are the same as in Table 2.1.

By comparing Fig. 3.12 and Fig. 3.13, it is shown that when orthogonal polarization state setting is used, CNR degradation is significantly reduced at the fiber length of 8.5 km, particularly for a large optical power. With the power of 1490-nm digital channel increasing from 0 to 4 dBm, shown in Fig. 3.12, the degradation of NRZ coding scheme increases from 1.1 to 4.4dB for parallel-aligned polarization states at the fiber input; however, shown in Fig. 3.13, the degradation of NRZ coding scheme increases from 0.2 to 1.1dB for orthogonal-aligned polarization states at the fiber input. It is possible to reduce up to ~3.3 dB by using orthogonal polarization states at fiber input when the

power of 1490 nm digital channel is 4 dBm.

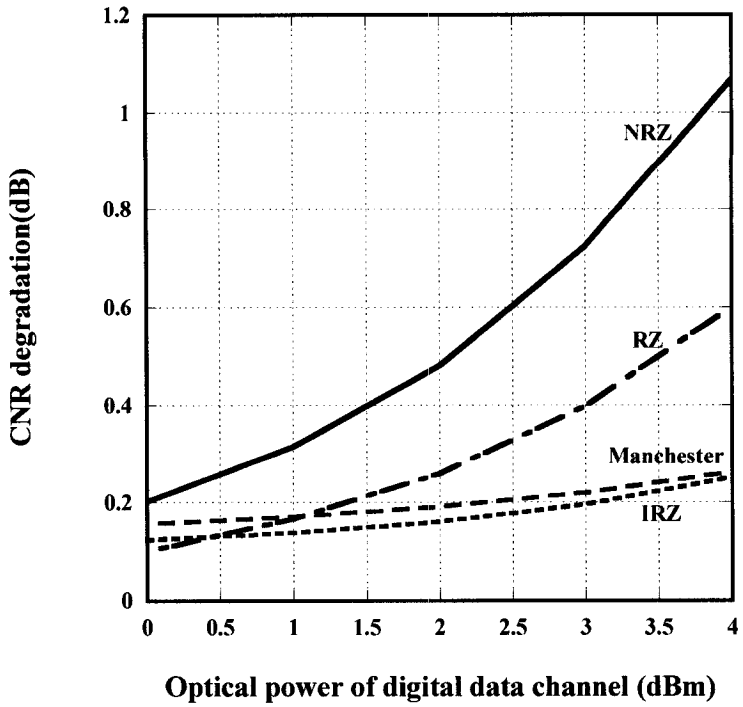

Fig. 3.13 - Raman crosstalk induced CNR degradation as a function of optical power of the digital data channel for orthogonal-aligned polarization states at the fiber input. The fiber length is 8.5 km with PMD of 0.1 $ps/\sqrt{km}$, and the others are the same as in Table 2.1.

3.3.3 Raman crosstalk induced CNR degradation as a function of optical modulation index of CATV channel

Corresponding to Fig. 3.7 and Fig. 3.8, Fig. 3.14 and Fig. 3.15 show CNR degradation due to Raman crosstalk as a function of optical modulation index considering fiber PMD impact. It is seen that Raman crosstalk induced CNR degradation is gradually reduced for NRZ, RZ, and IRZ by increasing optical modulation index of the optical RF

overlay channel as shown in Fig. 3.14. For Manchester, a small increase of optical modulation index does not help reduce the impact of Raman crosstalk. It is the same situation as shown in Fig. 3.7.

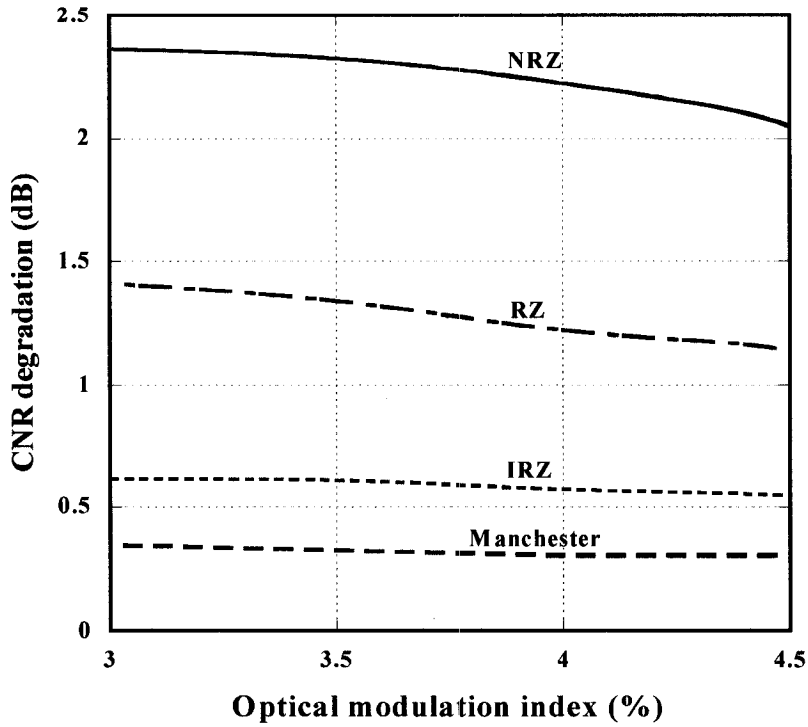

Fig. 3.14 - CNR degradation due to Raman crosstalk as a function of optical modulation index of the optical RF overlay channel for parallel-aligned polarization states at the fiber input. Optical power of the digital data channel is 2 dBm, the fiber length is 8.5 km with PMD of 0.1 $ps/\sqrt{km}$, and the others are the same as in Table 2.1.

As shown in Fig. 3.15, when polarization states are orthogonal-aligned at the fiber input and fiber PMD is included, a larger optical modulation index does help reduce the impact of Raman crosstalk for all NRZ, RZ, IRZ, and Manchester, particularly for NRZ and RZ. For example, a reduction of CNR degradation from 0.6 to 0.1 dB is induced by

increasing optical modulation index from 3 to 4.5% for NRZ.

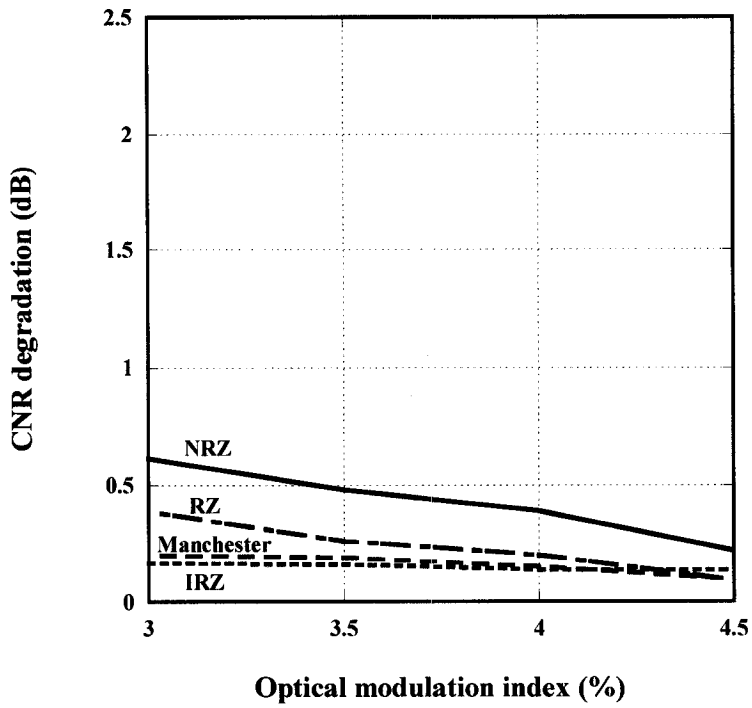

Fig. 3.15 - CNR degradation due to Raman crosstalk as a function of optical modulation index of the optical RF overlay channel for orthogonal-aligned polarization states at the fiber input. Optical power of the digital data channel is 2 dBm, the fiber length is 8.5 km with PMD of 0.1 $ps/\sqrt{km}$, and the others are the same as in Table 2.1.

3.4 CNR degradation due to laser RIN transfer

The pump to signal RIN transfer is one of the major issues in fiber Raman amplifier noise analysis [28]. In PON systems there is intensity modulation in the digital channel and the relative intensity noise (RIN) will transfer from the pump (optical digital channel at 1490nm) to the optical RF overlay signal at wavelength 1550 nm and degrade the CATV system CNR performance.

Because RIN transfer is directly proportional to the Raman crosstalk, we consider NRZ coding with the worst case because NRZ is the worst modulation format. Fig. 3.16 shows laser RIN transfer impact on CNR degradation for NRZ coding with fiber length of 8.5 km without consideration of fiber PMD, i.e. an ideal fiber. In Fig. 3.16 it is also assumed that parallel-aligned polarization states between the two optical channels are set at the fiber input. It is clearly shown in Fig. 3.16 that RIN transfer is has negligibly small on CNR even in the worst case.

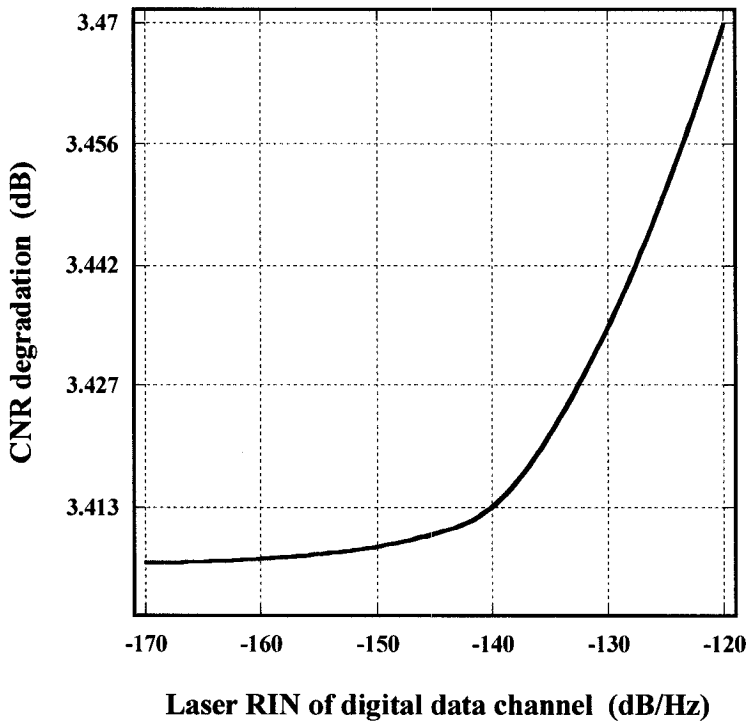

Fig. 3.16 - CNR degradation of NRZ coding due to RIN transfer with parallel-aligned polarization states at the fiber input without PMD. Optical power of the digital data channel is 2 dBm, fiber length is 8.5 km and the others are the same as in Table 2.1.

CHAPTER 4 CONCLUSIONS AND FUTURE WORKS

In the thesis, we investigate and analyze the impact of Raman crosstalk and RIN transfer on RF video overlay channels induced by 1490-nm optical intensity modulated digital data channel, considering modulation formats of non-return-to-zero (NRZ), return-to-zero (RZ), Inverse-RZ (IRZ), and Manchester coding, fiber length, optical power, optical modulation index and fiber polarization mode dispersion (PMD).

We evaluated Raman crosstalk induced CNR degradations in RF overlay channel of PON systems considering four coding schemes: NRZ, RZ, IRZ, and Manchester in chapter 3. Section 3.1 presents the spectral characteristic of Raman Crosstalk in RF overlay channel. Section 3.2 shows the investigation of Raman crosstalk induced CNR degradation with a virtual assumption that fiber has no PMD when polarization states of optical video overlay and digital channels maintain in parallel or orthogonal aligned along the fiber. For the worst case of Raman crosstalk, maximum CNR degradation due to Raman crosstalk can be up to 6, 4, and 2 dB for NRZ, RZ, and IRZ respectively depending on optical power of 1490-nm channel and negligibly small for Manchester. However, for the best case of Raman crosstalk, CNR degradation due to Raman crosstalk is very small and negligible. Section 3.3 illustrates Raman crosstalk with the consideration of PMD, i.e. real fiber. For this case, we investigate CNR degradation due to Raman crosstalk if polarization states along a fiber have random evolution due to PMD. Firstly, it is found that use of IRZ and Manchester coding schemes lead to a significant

reduction of Raman crosstalk, better than pre-emphasized RF power technique. Our investigation clearly shows that use of IRZ or Manchester will be the key technique for the reduction of Raman crosstalk because IRZ and Manchester are insensitive to 1490-nm optical power, fiber PMD, and RF power in Raman crosstalk. Furthermore, fiber PMD may reduce Raman crosstalk up to ~2 dB by using orthogonal polarization states at fiber input for NRZ and RZ at some fiber lengths, such as around 8.5 km, but for IRZ and Manchester the Raman crosstalk is hardly impacted by fiber PMD. For fiber length of more than 20 km, polarization state setting is almost useless due to fiber PMD. In Section 3.4 we evaluate RIN transfer impact on CNR. It is found that the impact of RIN transfer can be ignored in PON systems for both worst and best cases of Raman crosstalk.

There is still a lot of work to be done in this field.

First of all, there are still many coding schemes that we can use to shape the digital data channel power spectrum, such as phase shift key signal DPSK and multi-level signal DQPSK. Phase shift key and multi-level signaling is more like a CW than intensity modulated signal. This will definitely decrease Raman crosstalk in the lightwave system. However, it requires a more complex transceiver. The detailed comparison between optimal phase modulated signal like DPSK and multilevel signaling like DQPSK is desired concerning both system performance and commercial realization.

Last, so far, compensation for Raman crosstalk in PONs is done in optical domain. If we can find a way to compensate Raman crosstalk degradation electronically, the system design would be more flexible and more complicated signal processing in

electrical domain at transmitter/receiver end would be applied.

Reference:

[1] G. P. Agrawal, "Fiber-optic communication systems," 3rd edition, pp.4, 2002.

[2] H. Kogelnik, "IEEE J. Sel. Topics Quantum Electron." vol.6, pp.1279, 2000.

[3] G. P. Agrawal, "Lightwave Technology Telecommunication Systems," pp.404, 2005.

[4] G. Keiser, "FTTH Concepts and Applications," pp.4-5, 2006.

[5] G. Kramer, "Ethernet Passive Optical Networks," pp.10, 2005.

[6] J. George, "Designing passive optical networks for cost effective triple play support", OFS, FTTH Conference Orlando, FL, 2004.

[7] C. Raman and K. Krishnan, "A New Type of Secondary Radiation," Nature, vol.121, pp.501, 1928.

[8] M. Nissov, "Long-Haul Optical Transmission Using Distributed Raman Amplification," Ph.D. Thesis, Chapter 1, pp.2-13, December 1997.

[9] G. Agrawal, "Fiber-Optic Communication Systems" Chapter 2, pp.62, The Institute of Optics University of Rochester, Rochester, NY, third edition, 2002.

[10] F. Tian, R. Hui, B. Colella and D. Bowler, "Raman crosstalk in fober-optic hybrid CATV systems with wide channel separations," IEEE Photonics Technol. Lett., vol.16, pp.344-346, 2004.

[11] Q. Lin, and G. Agrawal, "Polarization mode dispersion induced fluctuations during Raman amplifications in optical fibers," OSA Optics Lett., vol. 27, pp.2194-2196, 2002.

[12] H. W. Hung, "An Optical Frequency-division Arrangement Scheme for The Improvement of CSO/CTB in Hybrid Fiber/Coaxial CATV System," Tung-Nan Junior College, 1999.

[13] C. Fludger, V. Handerek, and R. Mears, "Pump to signal RIN transfer in Raman fiber amplifiers," J. Lighwave Technol., vol.19, pp.1140-1148, 2001.

[14] "Cisco uBR7200 Series Universal Broadband Router Hardware Installation Guide Appendix E", Cisco Systems Inc., 2005.

[15] M. Philips, and D. Ott, "Crosstalk due to optical fiber nonlinearities in WDM CATV lightwave systems," J. Lightwave Technol., vol.17, pp.1782-1792, 1999.

[16] H. Kim, K. Han, and Y. Chung, "Performance limitation of hybrid WDM systems due to stimulated Raman scattering," IEEE Photonics Technol. Lett., vol.13, pp.1118-1120, 2001.

[17] F. Coppinger, L. Chen, and D. Piehler, "Nonlinear Raman cross-talk in a video overlay passive optical network", vol. 1, OFC, PP. 285-286, 2003.

[18] M. Aviles, K. Litvin, J. Wang, B. Colella, F. Effenberger, and F. Tian, "Raman crosstalk in video overlay passive optical networks," OFC, Vol. 2, Paper FE7, Los Angles, 2004.

[19] B. Colella, F. Effenberger, C. Shimer, and F. Tian, "Raman crosstalk control in passive optical networks," OFC Anaheim CA, Paper NWD6, 2006.

[20] F. Coppinger and D. Piehler, "RF video overlay in an Ethernet passive optical network," OFC Anaheim CA, Paper OThK7, 2006.

[21] "ITU-T Recommendation G.984.3 Amendment 2," ITU-T, March 2006.

[22] G. Lu et al, "Use of downstream inverse-RZ signal for upstream data re-modulation in a WDM passive optical network," OFI8, OSA 2005.

[23] W. Muys et al, "Mutual deterioration of WDM-coupled AM CATV and digital B_ISDN services in single fiber access network," IEEE Photon. Technol. Lett., Vol. 5 (7), pp. 832-834, 1993.

[24] J. Wang et al, "Mitigation of Raman crosstalk in BPON applications", FTTH council annual conference, Oct. 2004.

[25] J. Bromage, "Raman amplification for fiber communication systems," J. Lightwave Technol. Vol. 22, pp. 79-93, 2004.

[26] G. Keiser, "FTTH Concepts and applications", pp.39, 2006.

[27] A. Leung, "Performance Analysis of SCM Optical Transmission Link for Fiber-to-the-Home", Master Thesis, BSEE University of Missouri-Rolla, 2006.

[28] J. Zhou et al, "Frequency domain model to calculate the pump to signal RIN transfer in multi-pump Raman fiber amplifiers," Optics Express, Vol. 14, No. 23, 13 November 2006.